Human iPSC modeling elucidates mutation-specific responses to gene therapy in a genotypically diverse dominant maculopathy

Divya Sinha[1,2]*, Benjamin Steyer[1,3]*, Pawan K. Shahi[1,4], Katherine Mueller[3], Rasa Valiauga[2], Kimberly L. Edwards[2], Cole Bacig[2], Stephanie S. Steltzer[3], Sandhya Srinivasan[3], Amr Abdeen[3], Evan Cory[3], Viswesh Periyasamy[3], Alireza Fotuhi Siahpirani[3], Edwin M. Stone[5,6], Budd A Tucker[5,6], Sushmita Roy[3,7], Bikash R. Pattnaik[1,4,8]**, Krishanu Saha[1,3,9]**, David M. Gamm[1,2,8]**^

[1]McPherson Eye Research Institute, University of Wisconsin-Madison, Madison, WI, USA

[2]Waisman Center, University of Wisconsin-Madison, Madison, WI, USA

[3]Wisconsin Institute for Discovery, University of Wisconsin-Madison, Madison, WI, USA

[4]Department of Pediatrics, University of Wisconsin-Madison, Madison, WI, USA

[5]Department of Ophthalmology and Visual Sciences, Carver College of Medicine, Iowa City, IA

[6]Stephen A. Wynn Institute for Vision Research, University of Iowa, Iowa City, IA

[7]Department of Biostatistics, University of Wisconsin-Madison, Madison, WI, USA

[8]Department of Ophthalmology and Visual Sciences, University of Wisconsin-Madison, Madison, WI, USA

[9]Department of Biomedical Engineering, University of Wisconsin-Madison, Madison, WI, USA

* These authors contributed equally to the work

Co-Correspondence: D.M.G. (dgamm@wisc.edu), K.S. (ksaha@wisc.edu), and B. R. P. (pattnaik@wisc.edu)

^ **Lead contact:** D.M.G.

Subject Terms: human pluripotent stem cells, gene therapy, somatic cell gene editing, CRISPR-Cas9, gene augmentation, autosomal dominant disease, macular degeneration, orphan disease, channelopathy

SUMMARY

Dominantly inherited disorders are not typically considered therapeutic candidates for gene augmentation. Here we utilized patient iPSC-derived retinal pigment epithelium (iPSC-RPE) to test the potential of gene augmentation versus gene editing to treat Best disease, an autosomal dominant macular dystrophy caused by over 200 missense mutations. Gene augmentation restored calcium-activated chloride channel activity and improved rhodopsin degradation for a subset of dominant mutations depending on the putative role of the affected residue. In comparison, CRISPR-Cas9 editing of the mutant allele resulted in reversal of channel activity deficits for all mutations tested. Importantly, 95% of gene editing events in iPSC-RPE resulted in premature stop codons within the mutant allele, and single cell profiling demonstrated no adverse perturbation of RPE transcriptional programs. These results show that gene augmentation is a viable strategy for a subset of Best disease patients, and that non-responders are candidates for targeted editing of the mutant allele. Similar scenarios likely exist for other genotypically diverse dominant diseases, expanding the therapeutic landscape for patients.

INTRODUCTION

Genotypically heterogeneous dominant diseases pose significant challenges and opportunities for precision medicine (Doudna and Charpentier, 2014). Among gene therapies, gene augmentation for recessive disorders is the most developed, having spurred multiple clinical trials (Cukras et al., 2018; Lam et al., 2019; Russell et al., 2017) and FDA approval for one ocular disease (Ledford, 2017). However, gene augmentation is generally ruled out as a stand-alone therapy for dominant disorders due to a perceived need to eliminate the deleterious effects of the mutant allele. While gene editing holds promise in this regard (Bakondi et al., 2016; Li, 2018; Tsai et al., 2018), testing safety and efficacy for every mutant allele-targeted single guide RNA (sgRNA) presents practical and economic challenges. Further, gene editing may not be able to correct all mutations (Bakondi et al., 2016; Courtney et al., 2016; Pattanayak et al., 2013) and could lead to off-target mutagenesis—particularly within the heterozygous wildtype allele in dominant diseases—or other adverse events (Cromer et al., 2018). As such, it is prudent

to maximize use of gene augmentation in cases where it is deemed safe and efficacious and to reserve gene editing strategies for those patients who truly require it.

Best disease (BD), a common type of inherited macular degeneration, is a genotypically complex disorder transmitted primarily in an autosomal dominant fashion, although rare cases of autosomal recessive bestrophinopathy (ARB) are known (Johnson et al., 2017). Together, autosomal dominant Best disease (adBD) and ARB are linked to over 200 mutations in the *BEST1* gene. *BEST1* encodes a homo-pentameric calcium-activated chloride channel (CaCC) found in the RPE, a monolayer of cells essential for the survival and function of photoreceptors. While canine models of ARB closely mimic the human ARB phenotype (Guziewicz et al., 2017), no animal models of adBD exist. To provide a therapeutic testing platform for adBD, we previously developed the first human iPSC-RPE models of the disease, which demonstrated relevant cellular dysfunction; most notably, delayed degradation of phagocytosed photoreceptor outer segment (POS) proteins (Singh et al., 2015; Singh et al., 2013b). Recently, high-resolution crystal structures of Best1 were elucidated, which strongly supported its role as a CaCC (Dickson et al., 2014; Yang et al., 2014). Mutation hotspots in BEST1 were found to lie within calcium or chloride ion binding sites, or to contribute to the structural organization of the channel, among other putative roles (Dickson et al., 2014). Our two prior adBD iPSC-RPE models harbored mutations in a calcium binding (N296H) or structural (A146K) domain (Singh et al., 2015; Singh et al., 2013b). Therefore, for the present study, we generated iPSC-RPE from a third patient with adBD caused by a chloride binding site mutation (R218C), as well as an ARB patient with compound heterozygous mutations (R141H/A195V) (**Figure 1A**). We also employed RPE derived from two control lines: a wildtype (WT) iPSC line and an isogenic iPSC line generated via CRISPR-based gene correction of R218C adBD iPSCs (R218C>WT) (Steyer et al., 2018). Our findings suggest that certain mutations in *BEST1* are amenable to gene augmentation alone while others can be targeted via gene editing, contingent

on suitable sgRNA design. Furthermore, in the absence of suitable animal models, iPSC-derived RPE can serve as a robust preclinical platform for testing mutation-specific therapeutics.

RESULTS

BEST1 mutations decrease CaCC activity in patient-specific iPSC-RPE

The six iPSC lines were tested for pluripotency, differentiated to RPE, and characterized (**Figures 1 and S1A-D**). iPSC-RPE monolayers for all adBD and control lines, but not the ARB line, showed robust levels of BEST1 protein expression (**Figure 1D**). The profoundly decreased BEST1 level in our ARB cultures is consistent with reports using heterologous expression or iPSC-RPE systems that showed low or undetectable levels of R141H or A195V BEST1 (Marmorstein et al., 2018; Milenkovic et al., 2018). As a measurement of CaCC activity, single-cell patch clamp recordings of calcium-activated chloride current density were performed and found to be diminished in all patient-specific iPSC-RPE relative to WT control iPSC-RPE (**Figures 1E and S1E-I**). Gene-corrected R218C>WT isogenic iPSC-RPE control also showed CaCC current density at levels similar to native WT control lines (**Figures 1E and S1J**), confirming that the decreased CaCC activity is indeed the result of the mutation.

Virus-mediated *BEST1* augmentation restores CaCC activity and enhances rhodopsin degradation in ARB iPSC-RPE

We next sought to confirm that ectopic expression of wildtype human BEST1 (hBEST1) could ameliorate the disease phenotype of R141H/A195V ARB iPSC-RPE, analogous to gene augmentation studies using ARB canines or other iPSC-RPE model systems for ARB (Guziewicz et al., 2018; Li et al., 2017). Single-cell patch clamp recordings of calcium-activated chloride current density were used as a

readout of efficacy in iPSC-RPE cells. In addition, we monitored degradation of rhodopsin following POS feeding as an assay of intact RPE monolayer function.

For gene augmentation we used a lentivirus construct (*hVMD2-hBEST1-T2A-GFP*) designed to co-express hBEST1 and GFP under control of the human *BEST1* promoter (*hVMD2*), which assures both RPE-specific expression and *BEST1*-specific gene regulation (**Figures 2A and 2B**). Lentivirus was chosen for transgene delivery based on its safe use in human retinal gene therapy trials (Waugh et al., 2018) (ClinicalTrials.gov Identifiers: NCT01367444, NCT01736592) and its superior transduction efficiency in cultured human RPE (Pawan K. Shahi, 2019; Singh et al., 2013b). GFP expression was observed in ARB iPSC-RPE cells starting one week post-transduction, and immunocytochemical (ICC) and western blot analysis confirmed enhanced expression of BEST1 in treated cultures (**Figures 2C, S2A-C**). By ≥4 weeks post-transduction, CaCC current density in ARB iPSC-RPE increased significantly, reaching levels comparable to WT iPSC-RPE (**Figures 2D,E,J and S2E**). Furthermore, transduced monolayers of ARB iPSC-RPE demonstrated enhanced degradation of rhodopsin following POS feeding (**Figure 2F and S2I**). These findings, together with those reported by Guziewicz et al. (Guziewicz et al., 2018) and Li et al. (Li et al., 2017), support virus-mediated *hBEST1* gene augmentation as a treatment for ARB.

***BEST1* augmentation restores CaCC activity and enhances rhodopsin degradation for some—but not all—adBD iPSC-RPE**

Although not as intuitive, we also suspected that gene augmentation might be a viable solo therapeutic strategy for a subset of adBD-causing mutations. Based on the eukaryotic Best1 crystal structure, we hypothesized that mutations affecting chloride or calcium ion binding sites would not affect gross structure of the channel, but rather reduce its regulatory response and/or ion conductance capacity

proportional to the ratio of wildtype versus mutant monomers. If so, we would expect increased CaCC activity simply by shifting this ratio toward incorporation of more wildtype monomers through gene augmentation.

The *hVMD2-hBEST1-T2A-GFP* lentiviral construct was used to transduce iPSC-RPE from all three adBD patients (**Figure S2D**), which increased BEST1 expression in each line to a level comparable to that observed in gene augmented ARB-iPSC-RPE (**Figure 2G**). At ≥4 weeks post-transduction, CaCC activity was restored in iPSC-RPE containing mutations in a chloride (R218C) or a calcium (N296H) binding site, whereas iPSC-RPE harboring the A146K mutation, which resides in a structural domain of the channel, did not show restoration of CaCC activity (**Figure 2H,I,J and S2F-H**). Consistent with these single-cell electrophysiological findings, gene augmentation improved rhodopsin degradation in R218C and N296H iPSC-RPE, but not in A146K iPSC-RPE (**Figure 2K and S2J-L**).

Gene editing specifically targets the mutant allele in adBD iPSC-RPE with high efficiency and low off-target editing

To determine whether A146K iPSC-RPE would respond to an alternative therapeutic approach, we tested gene editing as a means to eliminate expression of the mutant *BEST1* allele. Gene editing with CRISPR-Cas9 creates targeted double strand breaks in genomic DNA that are primarily repaired by endogenous non-homologous end joining (NHEJ) (Cox et al., 2015), leading to insertion and deletion mutations (indels). These indels can cause transcriptional frameshifts that lead to premature termination codons, activation of intrinsic nonsense-mediated decay (NMD) pathways, and degradation of transcription products (Popp and Maquat, 2016).

We first tested gene editing in R218C iPSC-RPE given our previous success targeting the R218C mutant allele using CRISPR-Cas9, as well as the availability of an isogenic, fully gene-corrected control

iPSC line (R218C>WT) (Steyer et al., 2018). A specific sgRNA sequence targeting the R218C locus in the mutant allele was cloned into a lentiviral plasmid that encoded both the sgRNA (expressed via a U6 promoter) and a human codon optimized *Streptococcus pyogenes Cas9* (*spCas9)-T2A-GFP* transcript (expressed via a *VMD2* promoter) (**Figures 3A and 3B**). We also cloned a sgRNA control sequence targeting the *AAVS1* safe harbor locus (Sadelain et al., 2011) into the same lentiviral plasmid backbone to compare gene editing efficiency in iPSC-RPE from different lines. Transduction of R218C adBD iPSC-RPE and R218C>WT iPSC-RPE with the lentivirus encoding the *AAVS1* sgRNA revealed similarly robust and dose-dependent gene editing at the *AAVS1* locus (**Figure S3A**). We next assessed specificity of the R218C sgRNA for the mutant *BEST1* allele. R218C adBD iPSC-RPE and R218C>WT iPSC-RPE were transduced with the R218C sgRNA lentiviral genome editor. In R218C adBD iPSC-RPE, we observed a dose-dependent increase in percent edited alleles (maximum >20%) (**Figure 3C *right***); however, minimal (<2%) editing was detected in R218C>WT isogenic control iPSC-RPE (**Figure 3C *left***). This finding indicates that the R218C sgRNA efficiently and selectively edits the R218C mutant allele while leaving the WT allele nearly untouched, which is critical for therapeutic applications since concurrent disruption of the WT allele would likely worsen the adBD phenotype.

To test for off-target events after gene editing R218C adBD iPSC-RPE with the R218C sgRNA, we chose the lentiviral dose that yielded maximum editing (**Figure 3C)**. Analysis of the top nine off-target sites revealed measurable editing only at the second-ranked locus, which maps to an unannotated region on chromosome 7 (located 140 kb from any known coding region). Conversely, we observed remarkably efficient (24.9% ± 4.5% [SD]) editing at the on-target R218C *BEST1* locus in iPSC-RPE (**Figure 3D**), which equates to nearly half of all mutant alleles.

Gene editing as a therapeutic approach for adBD relies on both specific targeting of the mutant allele as well as introduction of indel mutations that result in premature termination of the mutant allele

transcript. Using deep sequencing, we examined specific indels that were introduced after gene editing R218C adBD iPSC-RPE (**Figure 3E *left***). In R218C iPSC-RPE edited with the R218C sgRNA lentiviral genome editor, an average of 94.5% of the edited alleles resulted in a frameshift mutation (**Figure 3E *right*; Table S1**). This frequency of out-of-frame indels is higher than that predicted from a recent machine learning algorithm (Shen et al., 2018) (**Table S1**), indicating a high likelihood that indels resulting from gene editing at the R218C locus will trigger NMD of the transcribed RNA.

To directly evaluate for NMD, we first quantified the average frequency of deep sequencing reads corresponding to WT, mutant, and edited alleles in genomic DNA isolated from R218C iPSC-RPE edited with R218C sgRNA or control (*AAVS1* sgRNA) lentiviral genome editor (**Figure 3F**). After editing with R218C sgRNA, there was a significant decrease in unedited R218C mutant allele frequency and a commensurate increase in edited R218C allele frequency. Importantly, no decrease in WT allele frequency was observed post-editing; rather, a small increase was found. However, this increase likely represents an artifact from large deletions in the edited mutant allele that are not detected by short read deep sequencing (Kosicki et al., 2018). This phenomenon has been observed previously with allele-specific genome editing (Li, 2018) and would result in an underestimation of the R218C mutant allele editing efficiency by our sequencing methodology. Together, these results reflect highly specific editing at the R218C mutant allele. After establishing genomic DNA editing efficiency, we sequenced RNA extracted from gene-edited R218C iPSC-RPE (**Figure S3B**). The ratio of WT to total mutant (R218C + edited R218C) RNA, but not genomic DNA reads, was increased in gene-edited versus control groups (**Figure S3C**). This finding is consistent with significant degradation of mutant allele transcripts after gene editing at the R218C allele, presumably through NMD.

Finally, we also evaluated the efficacy and specificity of gene editing in N296H iPSC-RPE and A146K iPSC-RPE. N296H and A146K mutant allele-targeted sgRNAs were designed and cloned into

separate lentiviral plasmids. N296H iPSC-RPE and A146K iPSC-RPE were transduced with lentiviral genome editors encoding either control (*AAVS1*) or corresponding allele-targeted sgRNA and editing outcomes were measured via deep sequencing (**Figure 3G-J**). As seen with R218C iPSC-RPE gene editing, a high proportion of editing in these two lines resulted in out-of-frame indels (96.0% and 95.4% for N296H and A146K iPSC-RPE, respectively), and further quantification of WT and mutant allele frequency indicated high specificity of the N296H and A146K sgRNAs to their respective mutant alleles.

Mutant allele-specific gene editing restores CaCC activity in iPSC-RPE derived from all tested adBD lines without perturbing global RPE transcriptional programs

We next assessed phenotypic rescue in control versus gene-edited iPSC-RPE using lentiviral genome editors expressing sgRNAs that target specific alleles. Single-cell patch clamp experiments revealed restoration of CaCC activity in R218C, N296H, and A146K iPSC-RPE cells (**Figures 4A-C and S4A-D**). To search for untoward transcriptional effects from gene editing, we performed single-cell RNA sequencing (scRNA-seq) for 12,061 individual iPSC-RPE cells treated with genome editors. iPSC-RPE (R218C, N296H, A146K, or isogenic control R218C>WT) were edited with genome editors encoding either a mutant allele-targeted sgRNA or a control sgRNA targeting *AAVS1*, to generate a total of eight separate samples (**Figure S4E-F**).

Evaluation of t-Distributed Stochastic Neighbor Embedding (t-SNE) clustering of cells across all eight samples indicated that, by virtue of using the *hVMD2* promoter, *spCas9-T2A-GFP* transcript levels closely corresponded with *BEST1* transcript levels (**Figure 4E**). Visual comparison of t-SNE clustering of each individual sample demonstrated that transcriptional signatures are grossly similar between iPSC-RPE lines whether treated with mutant allele-targeted (+GE) or control (*AAVS1*) sgRNA (**Figure 4F *top***). This observation was supported quantitatively by non-negative matrix factorization (NMF). NMF analysis

demonstrated that greater transcriptome variation exists between iPSC-RPE from different lines than between iPSC-RPE from the same line treated with mutant allele-targeted or control sgRNA (**Figure S4F**).

Additional analysis of global gene expression (**Figure 4F *bottom***) and of a focused set of genes related to negative or off-target effects (including cell cycle regulation, apoptosis, DNA damage response, or innate immune response; **Figure S4G, Table S2**) did not reveal significant upregulation of those gene sets in mutant allele-targeted (+GE) versus control sgRNA-treated samples.

DISCUSSION

The observation that adBD mutations associated with ion binding may be amenable to gene augmentation greatly expands the patient population that might benefit from this therapeutic approach. Among the over 200 known *BEST1* mutations, many are predicted to be directly or indirectly involved in ion binding (Boon et al., 2009; Dickson et al., 2014). However, the stark difference in functional response to gene augmentation among our adBD iPSC-RPE models underscores the need to vet patient candidacy for gene augmentation carefully.

The mechanism underlying selective responsivity of adBD patients to gene augmentation cannot be due to traditional allelic haploinsufficiency, in which half the normal amount of WT protein and no mutant protein is produced, resulting in fewer (but fully WT) BEST1 channels. Such a situation exists in parents of ARB patients, who have no demonstrable disease phenotype. Rather, adBD mutant monomers must be incorporated alongside WT monomers in all (or nearly all) BEST1 channels (Johnson et al., 2014). In the case of R218C and N296H, this would selectively cause ion binding site insufficiency and channel impermeability, a condition that is surmountable by WT *BEST1* augmentation. In contrast, we hypothesize that *BEST1* mutations like A146K—which converts a nonpolar amino acid to a polar amino

acid in a structural region of the protein—has more pervasive functional consequences, resulting in resistance to gene augmentation.

Importantly, we showed that BEST1 protein levels were equivalent across all lines following gene augmentation. Thus, the differences in functional response observed between R218C or N296H adBD iPSC-RPE and A146K adBD iPSC-RPE cannot be due to variability in transgene expression. It is also notable that our lentiviral constructs employed the *hVMD2* promoter, which is ideal from a translational standpoint as it specifies expression in RPE and supports native regulation of *BEST1*. Use of alternative promoters poses risks of off-target cell effects and/or undesirably low (ineffectual) or high (toxic) levels of protein expression. For construct delivery, we selected lentivirus based on its current use in RPE gene therapy trials and its excellent *in vitro* RPE transduction efficiency. However, our findings are applicable across all *in vivo* transgene delivery platforms that possess comparable safety and transduction profiles.

There is precedence for using patient-specific iPSCs as preclinical efficacy models for gene therapy (Vasireddy et al., 2013). Our work extends this utility by providing a framework for preclinical testing of mutation-specific responses in a genotypically heterogenous disease using the affected cell type. It remains to be determined whether separate adBD iPSC-RPE models will be required to assess suitability of gene augmentation versus gene editing for every mutation, or if a few models can sufficiently represent larger categories of mutations (*e.g.*, ion binding sites or structural regions).

For adBD mutations like A146K that are not amenable to gene augmentation, we showed that targeted gene editing holds great promise as a future therapy. Indeed, there is a wide spectrum of *BEST1* mutations that potentially could be treated by CRISPR-Cas9 by designing appropriate sgRNAs (examples shown in **Table S4**). While other gene therapy strategies also exist for dominant ocular diseases, they are often conceptually more complex, requiring knockdown of both wildtype and mutant allele transcripts with simultaneous introduction of a modified wildtype gene (Cideciyan et al., 2018). Whether such an

approach would be safe and effective for adBD mutations that fail to respond to straightforward gene augmentation is not known.

In our gene editing experiments, we observed higher efficiency out-of-frame editing in iPSC-RPE when compared to a prior study using undifferentiated iPSCs (Steyer et al., 2018). This finding is consistent with recent reports of variable mutation bias across different cell types (Shen et al., 2018), and points to the importance of evaluating gene editing using the specific cell type(s) targeted by disease, and not surrogate cell types. In addition, editing at *BEST1* in iPSC-RPE did not provoke an increase in expression of genes associated with cell cycle regulation, apoptosis, DNA damage response, or innate immune response in comparison to editing at a well characterized safe-harbor locus (Sadelain et al., 2011) with a previously described sgRNA (Mali et al., 2013). This result is in contrast to studies in other cell types that have reported potential for Cas9-mediated gene editing to provoke undesirable effects, including innate immune response (Wienert et al., 2018) and apoptosis, among other concerns (Cromer et al., 2018).

Our results provide a blueprint to guide gene therapy choice in the era of gene augmentation and gene editing. With its inherently larger target populations and established track record in patients, it is practical to utilize gene augmentation when possible, reserving gene editing for mutations that require allele repair or knockout or are otherwise untreatable by gene augmentation. It is noteworthy that the two adBD lines that demonstrated restoration of CaCC activity with gene augmentation or gene editing did so with equal efficacy, underscoring the suitability of Best disease for either approach. Other desirable characteristics of Best disease as a clinical candidate for gene augmentation or gene editing include 1) a wide time window for gene therapy intervention, 2) accessibility of RPE using standard surgical techniques, 3) a small (5.5 mm diameter) treatment area, 4) availability of noninvasive retinal imaging and functional assessment tools, and 5) growing patient safety data from other RPE-based gene therapy

trials (Cukras et al., 2018; Lam et al., 2019; Russell et al., 2017). As such, Best disease is well-positioned to become the first genotypically heterogeneous disorder with dominant and recessive inheritance patterns to have a full menu of therapeutics for all affected individuals. Furthermore, implications of this work likely extend beyond the eye and Best disease to other intractable monogenic conditions caused by mutations in multimeric ion channels, including congenital myasthenic syndromes and some forms of epilepsy (George, 2004; Schaaf, 2014; Villa and Combi, 2016).

ACKNOWLEDGEMENTS

The authors thank Alfred Lewin (U. Florida) for the *hVMD2-hBEST1-T2A-GFP* plasmid construct; the Cellular Imaging and Analysis core at the University of Wisconsin-Madison Waisman Center; and Andrew Thliveris for helpful discussions. This work was supported by NIH R01EY024588 (to D.M.G., B.A.T., and E.M.S.); Foundation Fighting Blindness, Research to Prevent Blindness, Retina Research Foundation Emmett Humble Chair, and McPherson Eye Research Institute Sandra Lemke Trout Chair in Eye Research (to D.M.G.); NSF CBET-1350178 and CBET-1645123, NIH R35GM119644, John Merck Fund Translational Research Program, Brain & Behavior Research Foundation, Burroughs Wellcome Fund (to K.S.); NIH R01EY024995 and Retina Research Foundation M.D. Mathews Professorship (to B.R.P.); NIH T32HG002760 and F30EY027699, VitreoRetinal Surgery Foundation (to B.S.); DGE-1747503 (to K.M.). This study was supported in part by a core grant to the Waisman Center (NICHHD U54 HD090256). We thank members of the Gamm and Saha labs for comments on the manuscript, plasmid depositors to Addgene, the University of Wisconsin-Madison Biotechnology Center for DNA sequencing, and the University of Wisconsin-Madison Skin Disease Research Center for assistance with virus preparation.

AUTHOR CONTRIBUTIONS

D.S. and D.M.G. designed the gene augmentation experiments. B.S., D.S., D.M.G. and K.S. designed the gene editing experiments. P.K.S. and B.R.P. performed and analyzed the electrophysiology experiments. D.S. and B.S. performed all other experiments with contributions from R.V., K.L.E., C.B, S.S.S., A.A., and E.C. K.M., S.S., V.P., A.F.S., and S.R. were primarily responsible for the scRNA-seq analysis. B.A.T. and E.M.S. provided and characterized the ARB iPSC line, D.S., B.S., K.S., and D.M.G. wrote the manuscript and analyzed data with input from all authors. D.M.G., K.S., and B.R.P. supervised research.

COMPETING INTERESTS STATEMENT

The authors declare no competing interests.

GRAPHICAL ABSTRACT

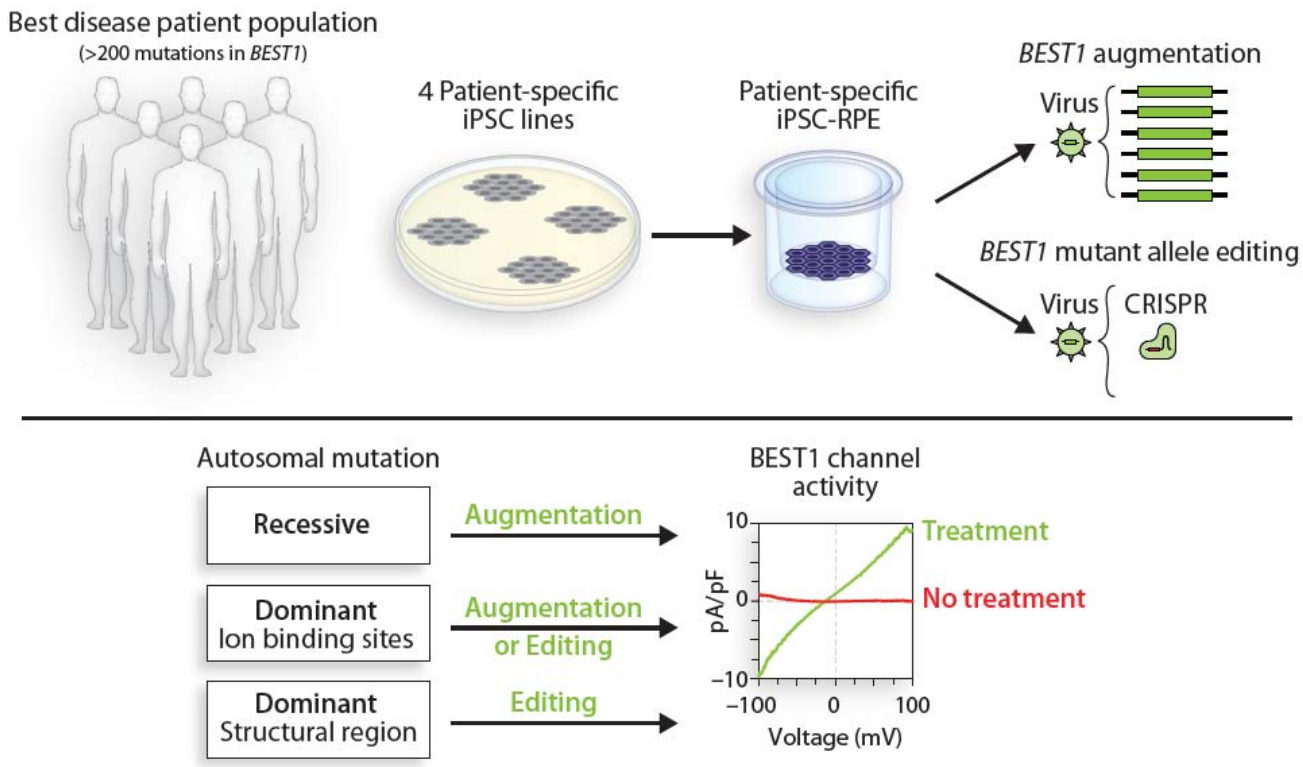

FIGURES AND FIGURE LEGENDS

Figure 1

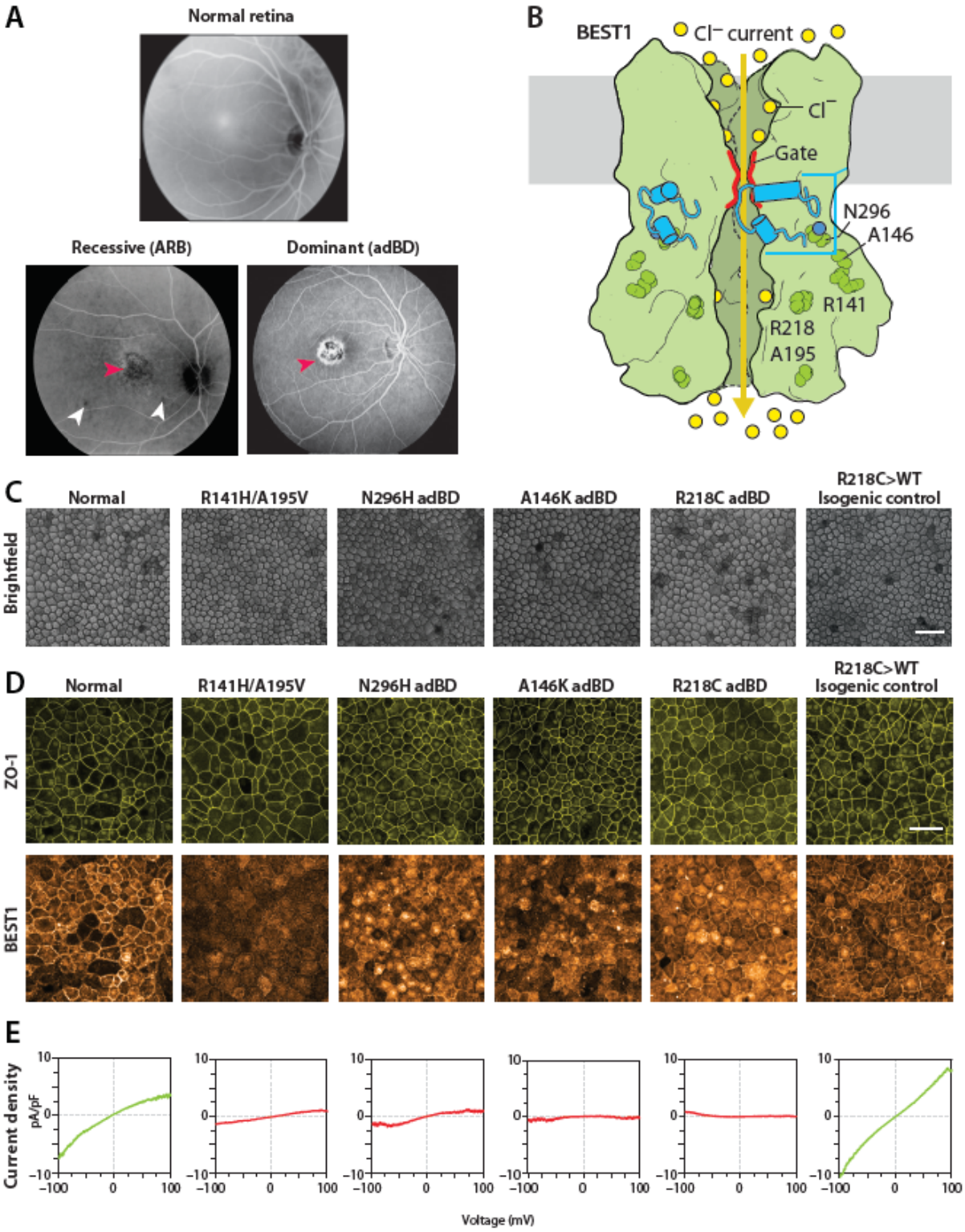

Figure 1 | *BEST1* mutations reduce CaCC current in Best disease iPSC-RPE. (A) *top*, image (in grayscale) of a normal fundus; *bottom left*, fundus image of an ARB patient with R141H/A195V compound heterozygous mutations in *BEST1* showing a vitelliform lesion in the macula (*red* arrowhead) as well as small lesions outside the macula (*white* arrowheads); *bottom right*, fundus image showing a vitelliform macular lesion (*red* arrowhead) in an adBD patient with a heterozygous R218C encoding mutation in *BEST1*. **(B)** A fully functional homo-pentameric BEST1 channel is formed by assembly of WT subunits (*green*), allowing movement of chloride ions (*yellow* circles) upon binding of calcium ions (*blue* circle) (based on the eukaryotic Best1 crystal structure (Dickson et al., 2014)). **(C)** Light microscopic images of normal, patient-specific, and isogenic control iPSC-RPE used in this study. Scale bar = 50 µm (applies to all images in C). **(D)** Immunocytochemical analyses of ZO-1 and BEST1 protein expression in iPSC-RPE cells. Scale bar = 50 µm (applies to all images in D). **(E)** CaCC current density-voltage plots from WT, R141H/A195V ARB, or adBD iPSC-RPE cells (identical order as in panels C and D), as determined by calculating the difference in average chloride currents in the presence or absence of calcium (Figure S1). For +calcium: n = 6 cells for WT, 12 cells for R141H/A195V ARB, and 5 cells for R218C adBD; for no calcium: n = 8 cells for WT, 12 cells for R141H/A195V ARB, and 8 cells for R218C adBD (data combined from at least two replicates).

Figure 2

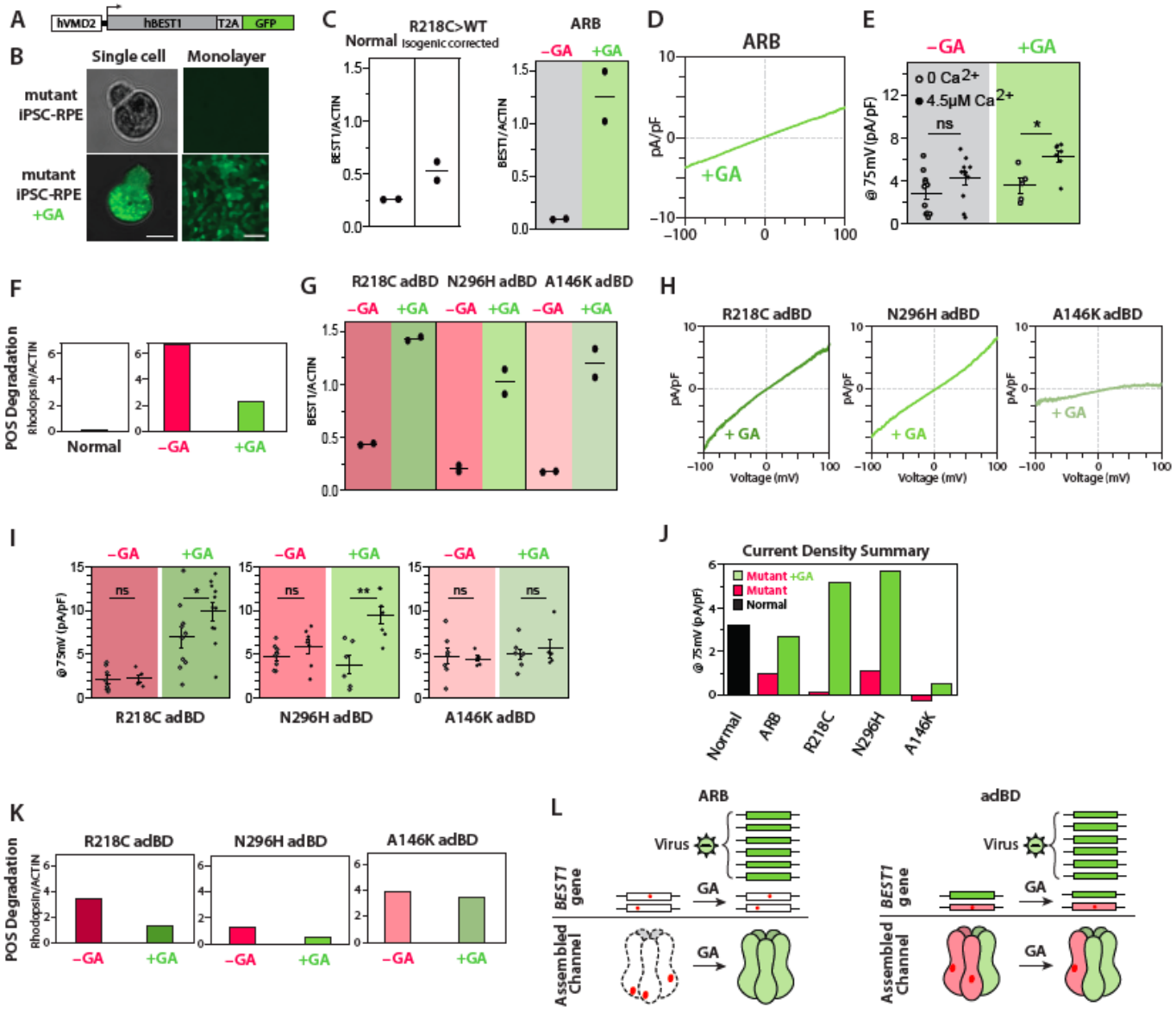
A
hVMD2
hBEST1
T2A
GFP
B
Single cell
Monolayer
mutant iPSC-RPE
mutant iPSC-RPE +GA
C
R218C>WT
Normal
Isogenic corrected
ARB
−GA
+GA
BEST1/ACTIN
D
ARB
pA/pF
+GA
E
−GA
+GA
0 Ca2+
4.5μM Ca2+
ns
*
@ 75mV (pA/pF)
F
POS Degradation
Rhodopsin/ACTIN
Normal
−GA
+GA
G
R218C adBD
N296H adBD
A146K adBD
BEST1/ACTIN
H
R218C adBD
N296H adBD
A146K adBD
pA/pF
+ GA
Voltage (mV)
I
−GA
+GA
ns
*
**
@ 75mV (pA/pF)
R218C adBD
N296H adBD
A146K adBD
J
Current Density Summary
Mutant +GA
Mutant
Normal
@ 75mV (pA/pF)
Normal
ARB
R218C
N296H
A146K
K
POS Degradation
Rhodopsin/ACTIN
R218C adBD
N296H adBD
A146K adBD
−GA
+GA
L
ARB
adBD
Virus
GA
BEST1 gene
Assembled Channel

Figure 2 | Mutation-dependent rescue of Best disease phenotypes by gene augmentation (GA). (A) Construct used for BEST1 gene augmentation. **(B)** Presence or absence of GFP fluorescence in a single dissociated iPSC-RPE cell (*left*) or iPSC-RPE monolayers (*right*) before (*top*) or after (*bottom*) gene augmentation. Scale bar = 10 µm (*left*); 50 µm (*right*). **(C)** Western blot-based quantification of BEST1 protein levels (normalized to ACTIN) in WT iPSC-RPE, ARB iPSC-RPE, and ARB iPSC-RPE after *BEST1* augmentation. **(D)** CaCC current density-voltage plots after gene augmentation of ARB iPSC-RPE. n = 7 cells for +calcium and 5 cells for no calcium (data combined from two replicates (Figure S2). **(E)** CaCC conductance for individual ARB iPSC-RPE cells at 75 mV before or after gene augmentation. The number of cells is the same as for panels 1E and 2D. **(F)** Western blot-based quantification of rhodopsin levels 120 hr after photoreceptor outer segment (POS) feeding in WT iPSC-RPE, ARB iPSC-RPE, and ARB iPSC-RPE after *BEST1* augmentation. **(G)** Western blot-based quantification of BEST1 protein levels (normalized to ACTIN) in adBD iPSC-RPE before and after *BEST1* augmentation. **(H)** CaCC current density-voltage plots after gene augmentation of adBD iPSC-RPE. For +calcium: n = 11 cells for R218C, 7 cells for N296H, and 5 cells for A146K; for no calcium: n = 9 cells for R218C, 6 cells for N296H, and 8 cells for A146K (data combined from two replicates). **(I)** CaCC conductance for individual adBD iPSC-RPE cells at 75 mV before and after gene augmentation. The number of cells is the same as for panels 1E and 2H. **(J)** Mean CaCC conductance at 75 mV before or after gene augmentation for all iPSC-RPE tested. **(K)** Rhodopsin levels 48 hours after feeding POS to adBD iPSC-RPE with or without gene augmentation. **(L)** Model to illustrate gene augmentation findings in ARB and adBD iPSC-RPE. Error bars in 2E and 2I represent mean ± SEM; ns = $p \geq 0.05$, * for $p < 0.05$, ** for $p < 0.01$. Western blots used for quantification are shown in Figure S2.

Figure 3

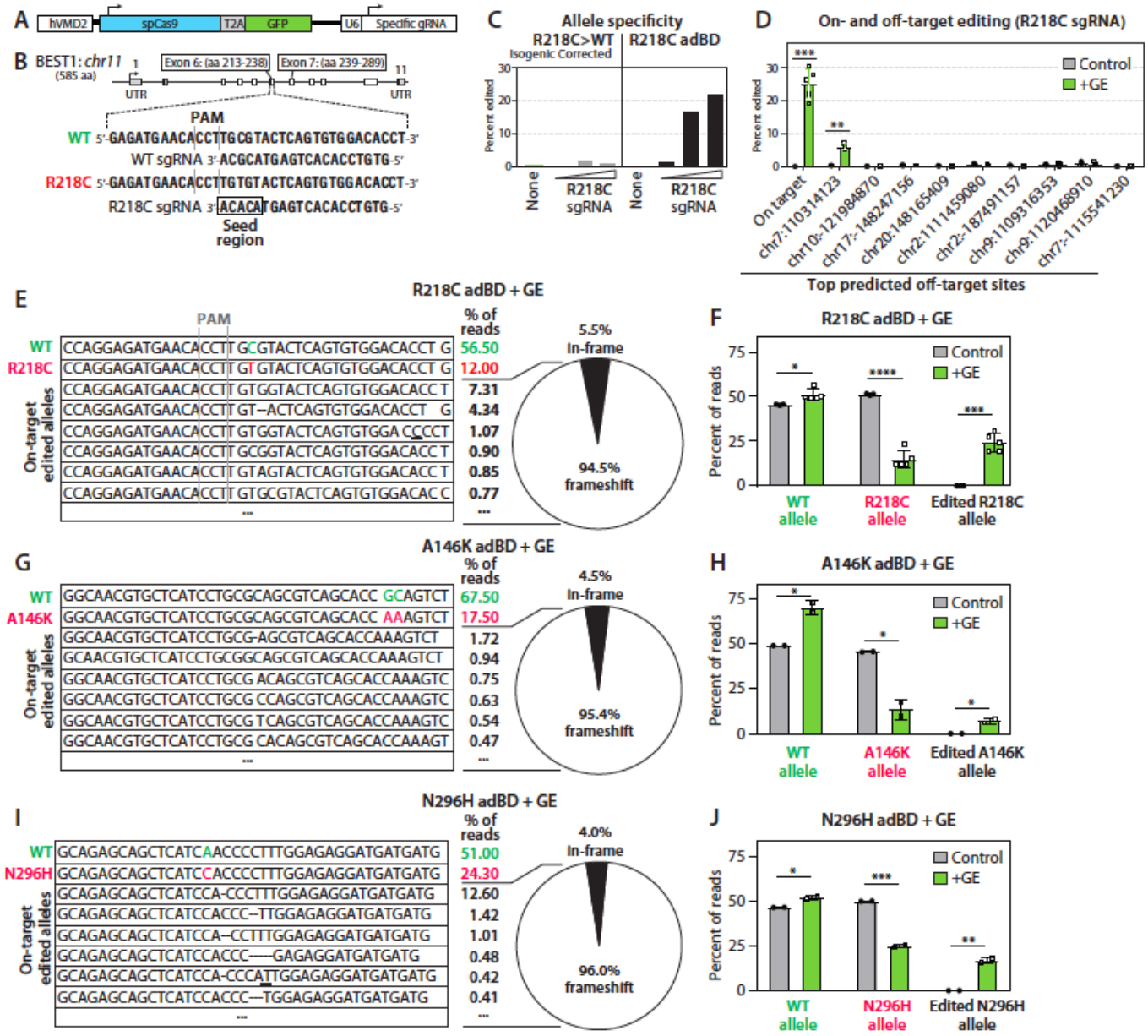
A
hVMD2
spCas9
T2A
GFP
U6
Specific gRNA
B
BEST1: chr11
(585 aa)
Exon 6: (aa 213-238)
Exon 7: (aa 239-289)
UTR
UTR
PAM
WT 5'-GAGATGAACACCTTGCGTACTCAGTGTGGACACCT-3'
WT sgRNA 3'-ACGCATGAGTCACACCTGTG-5'
R218C 5'-GAGATGAACACCTTGTGTACTCAGTGTGGACACCT-3'
R218C sgRNA 3'-ACACATGAGTCACACCTGTG-5'
Seed region
C
Allele specificity
R218C>WT
Isogenic Corrected
R218C adBD
Percent edited
None
R218C sgRNA
None
R218C sgRNA
D
On- and off-target editing (R218C sgRNA)
Control
+GE
Percent edited
On target
chr7:110314123
chr10:-121984870
chr17:-148247156
chr20:148165409
chr2:111145909080
chr2:-187491157
chr9:110931653
chr9:112046891 0
chr7:-111554123 0
Top predicted off-target sites
E
R218C adBD + GE
PAM
% of reads
WT CCAGGAGATGAACACCTTGCGTACTCAGTGTGGACACCTG 56.50
R218C CCAGGAGATGAACACCTTGTGTACTCAGTGTGGACACCTG 12.00
On-target edited alleles
CCAGGAGATGAACACCTTGTGGTACTCAGTGTGGACACCT 7.31
CCAGGAGATGAACACCTTGT--ACTCAGTGTGGACACCTG 4.34
CCAGGAGATGAACACCTTGTGGTACTCAGTGTGGACCCCT 1.07
CCAGGAGATGAACACCTTGCGGTACTCAGTGTGGACACCT 0.90
CCAGGAGATGAACACCTTGTAGTACTCAGTGTGGACACCT 0.85
CCAGGAGATGAACACCTTGTGCGTACTCAGTGTGGACACC 0.77
5.5% In-frame
94.5% frameshift
F
R218C adBD + GE
Control
+GE
Percent of reads
WT allele
R218C allele
Edited R218C allele
G
A146K adBD + GE
% of reads
WT GGCAACGTGCTCATCCTGCGCAGCGTCAGCACC GCAGTCT 67.50
A146K GGCAACGTGCTCATCCTGCGCAGCGTCAGCACC AAAGTCT 17.50
On-target edited alleles
GGCAACGTGCTCATCCTGCG-AGCGTCAGCACCAAAGTCT 1.72
GCAACGTGCTCATCCTGCGGCAGCGTCAGCACCAAAGTCT 0.94
GGCAACGTGCTCATCCTGCG ACAGCGTCAGCACCAAAGTC 0.75
GGCAACGTGCTCATCCTGCG CCAGCGTCAGCACCAAAGTC 0.63
GGCAACGTGCTCATCCTGCG TCAGCGTCAGCACCAAAGTC 0.54
GGCAACGTGCTCATCCTGCG CACAGCGTCAGCACCAAAGT 0.47
4.5% In-frame
95.4% frameshift
H
A146K adBD + GE
Control
+GE
Percent of reads
WT allele
A146K allele
Edited A146K allele
I
N296H adBD + GE
% of reads
WT GCAGAGCAGCTCATCAACCCCTTTGGAGAGGATGATGATG 51.00
N296H GCAGAGCAGCTCATCCACCCCTTTGGAGAGGATGATGATG 24.30
On-target edited alleles
GCAGAGCAGCTCATCCA-CCCTTTGGAGAGGATGATGATG 12.60
GCAGAGCAGCTCATCCACCC--TTGGAGAGGATGATGATG 1.42
GCAGAGCAGCTCATCCA--CCTTTGGAGAGGATGATGATG 1.01
GCAGAGCAGCTCATCCACCC----GAGAGGATGATGATG 0.48
GCAGAGCAGCTCATCCA-CCCATTGGAGAGGATGATGATG 0.42
GCAGAGCAGCTCATCCACCC---TGGAGAGGATGATGATG 0.41
4.0% In-frame
96.0% frameshift
J
N296H adBD + GE
Control
+GE
Percent of reads
WT allele
N296H allele
Edited N296H allele

Figure 3 | Gene editing (GE) specifically and efficiently introduces frameshifts within the mutant allele in adBD iPSC-RPE. (A) Lentiviral genome editing construct expressing *sp*Cas9 and mutant allele-targeted sgRNAs. **(B)** Diagram showing the heterozygous base pair substitution in R218C adBD and the design of the R218C sgRNA. **(C)** Percent of edited alleles after treatment of R218C>WT isogenic control iPSC-RPE and R218C adBD iPSC-RPE with R218C sgRNA lentiviral genome editor (single replicate at 0, 5, 50, or 150 µl dose). **(D)** Frequency of edited alleles at on-target and top nine ranked off-target loci in iPSC-RPE treated with R218C sgRNA lentiviral genome editor (n=3 for control and n=5 for +GE, except n=3 at *chr 7* locus). **(E, G, I)** Representative deep sequencing reads after treatment of R218C, A146K, or N296H iPSC-RPE with R218C sgRNA, A146K sgRNA, or N296H sgRNA lentiviral genome editor, respectively; and corresponding average indel frameshift frequency for iPSC-RPE (two replicates per line; data shown in Table S1). **(F, H, J)** Percentage of WT, unedited mutant, or edited mutant allele sequencing reads in R218C, A146K or N296H iPSC-RPE treated with R218C sgRNA, A146K sgRNA, or N296H sgRNA lentiviral genome editor, respectively. Replicates: n = 5 (R218C iPSC-RPE); n = 2 (A146K IPSC-RPE and N296H RPE). Error bars represent mean ± SD; ns = $p \geq 0.05$, * for $p < 0.05$, ** for $p < 0.01$, *** for $p < 0.001$, **** for $p < 0.0001$.

Figure 4

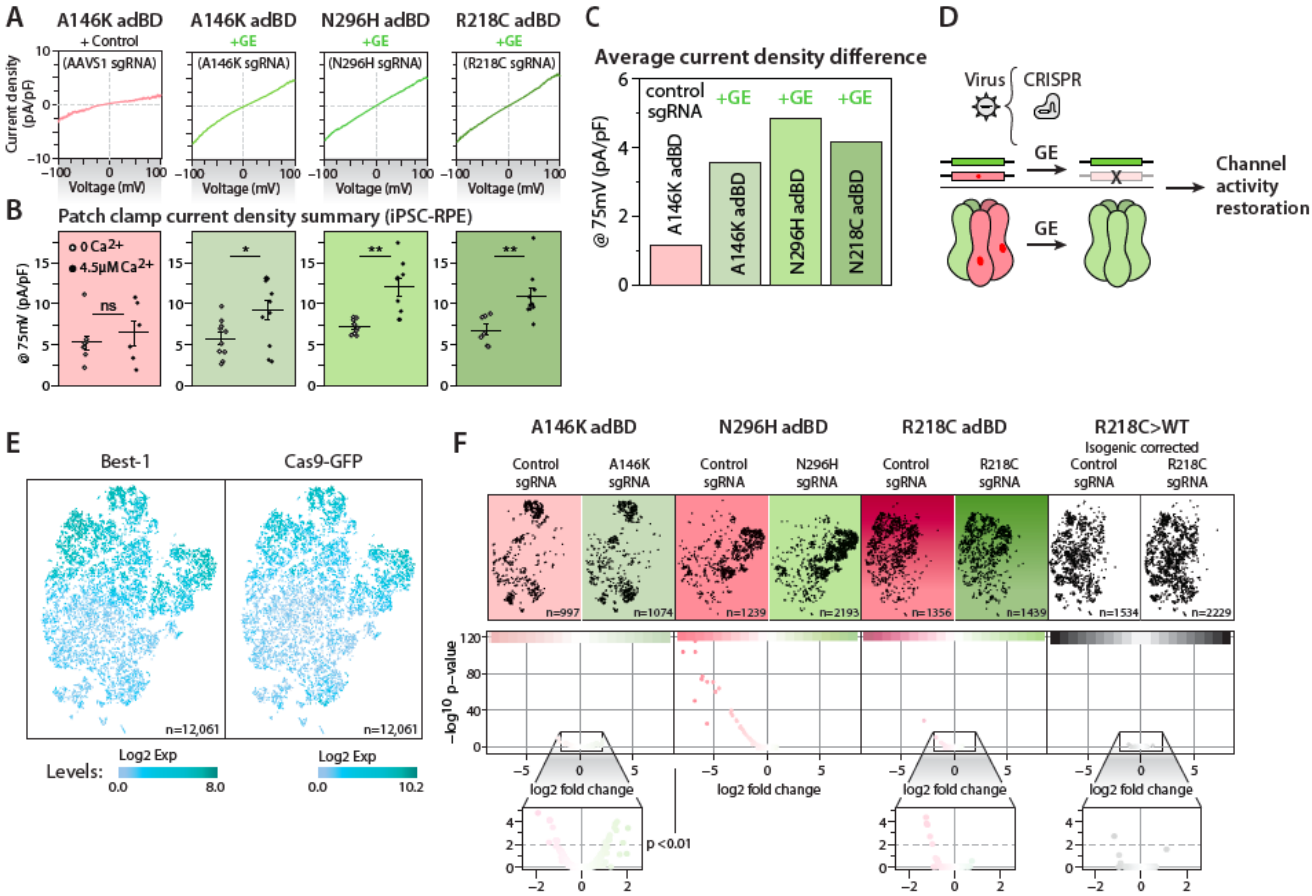
A
A146K adBD
+ Control
(AAVS1 sgRNA)
A146K adBD
+GE
(A146K sgRNA)
N296H adBD
+GE
(N296H sgRNA)
R218C adBD
+GE
(R218C sgRNA)
Current density (pA/pF)
Voltage (mV)
B
Patch clamp current density summary (iPSC-RPE)
0 Ca2+
4.5μM Ca2+
ns
@ 75mV (pA/pF)
C
Average current density difference
control sgRNA
+GE
A146K adBD
N296H adBD
R218C adBD
@ 75mV (pA/pF)
D
Virus
CRISPR
GE
Channel activity restoration
E
Best-1
Cas9-GFP
n=12,061
Levels:
Log2 Exp
0.0
8.0
10.2
F
A146K adBD
N296H adBD
R218C adBD
R218C>WT
Isogenic corrected
Control sgRNA
A146K sgRNA
N296H sgRNA
R218C sgRNA
n=997
n=1074
n=1239
n=2193
n=1356
n=1439
n=1534
n=2229
−log10 p−value
log2 fold change
p <0.01

Figure 4 | Gene editing (GE) rescues CaCC activity in adBD iPSC-RPE without disrupting RPE transcriptional identity. (A) CaCC current density-voltage plots from single-cell patch clamp experiments of iPSC-RPE treated with control (*AAVS1*) or mutant allele-targeted sgRNA lentiviral genome editor. For +calcium: n = 6 cells for *AAVS1*, 11 cells for A146K, 10 cells for R218C, 9 cells for N296H; for no calcium: n = 9 cells for *AAVS1*, 10 cells for A146K, 7 cells for R218C, 9 cells for N296H (data combined from two replicates). **(B)** CaCC conductance for individual iPSC-RPE cells, and **(C)** mean CaCC conductance at 75 mV. The number of cells is the same as for panel A. **(D)** Model depicting postulated effects of mutant allele-targeted gene editing in adBD iPSC-RPE. **(E)** t-SNE plot of single iPSC-RPE cells across all 8 samples with relative expression of *BEST1* (*left*) and *spCas9-T2A-GFP* (*right*) depicted via increasing shades of *blue*. Total number of cells analyzed (n) is shown. **(F)** *Top*, t-SNE plot of single cells (*black* dots) from each treated sample. Number of cells analyzed (n) for each sample is shown. *Bottom*, Volcano plots of transcriptome-wide differences in expression of individual genes (*red* or *green* dots) between iPSC-RPE of the same genotype treated with mutant allele-targeted sgRNA (*green*) versus control (*AAVS1*, *red*) sgRNA lentiviral genome editor. $p < 0.01$ was the threshold for determining significant versus non-significant changes in gene expression. Error bars in 4B represent mean ± SEM. * for $p < 0.05$, and ** for $p < 0.01$.

Figure S1. Related to Figure 1

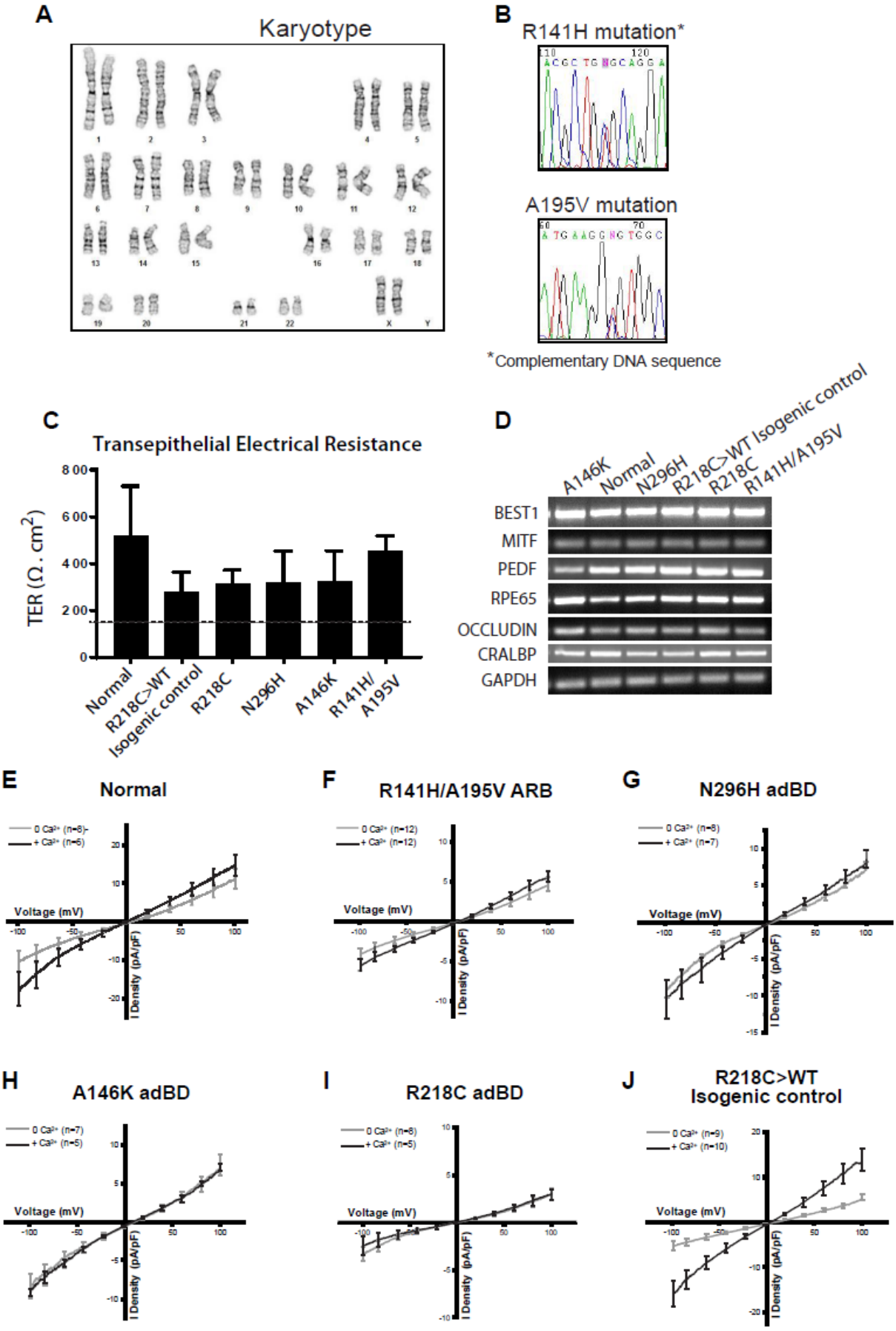

Figure S1 | Characterization of iPSC-RPE. (A) Karyotype analysis for ARB iPSCs. **(B)** DNA sequencing confirming R141H and A195V encoding mutations in ARB iPSCs. **(C)** Net transepithelial electrical resistance (TER) ($\Omega \cdot cm^2$) for iPSC-RPE from all six lines. The dashed line demarcates the minimum expected TER (150 $\Omega \cdot cm^2$). Replicates: n=12 for each line (4 transwells from 3 replicates each), error bars represent mean ± SD. **(D)** Gene expression analysis (RT-PCR) of selected RPE-specific markers in all six lines. **(E-J)** Chloride current traces, measured in the presence (*black*) or absence (*gray*) of calcium over a voltage ramp (-100 to +100 mV), that were used to generate CaCC current density plots in Figure 1E. 4.5 µM calcium was used for +calcium conditions. The number (n) of individual cells patch clamped in the presence or absence of calcium in order to calculate CaCC current densities is shown in the top left corner of each graph. Data were obtained from at least two replicates.

Figure S2. Related to Figure 2

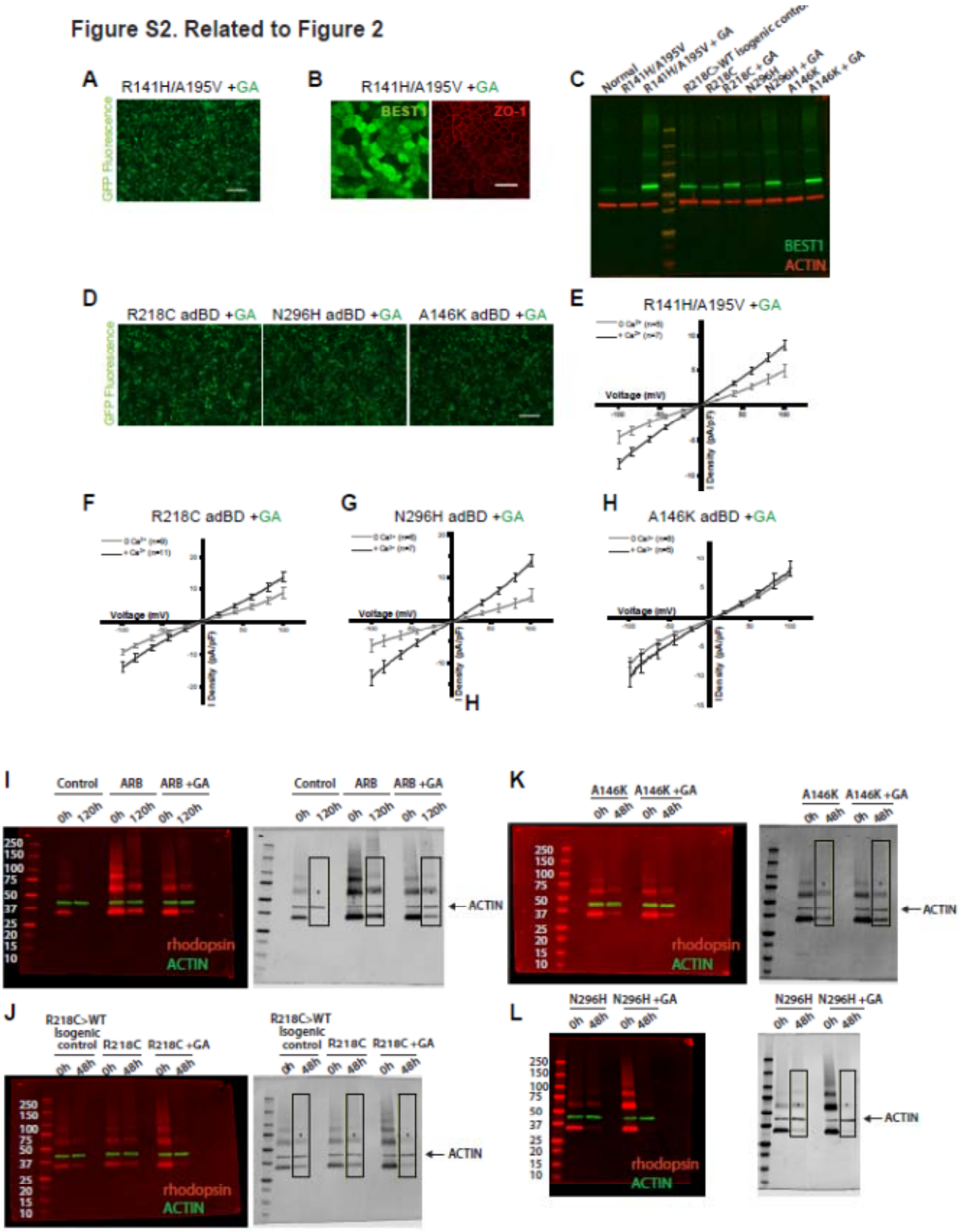

433

Figure S2 | Gene augmentation (GA) restores CaCC function in ARB iPSC-RPE and R218C and N296H adBD iPSC-RPE, but not in A146K adBD iPSC-RPE. (A) GFP fluorescence in R141H/A195V ARB iPSC-RPE transduced with lentivirus expressing BEST1. Scale bar = 100 µm. **(B)** ICC analysis of BEST1 and ZO-1 expression in R141H/A195V iPSC-RPE transduced with lentivirus expressing BEST1. Increased BEST1 expression is observed in R141H/A195V iPSC-RPE cells following gene augmentation. Scale bar = 50 µm (applies to both images). **(C)** Representative western blot showing levels of BEST1 in iPSC-RPE. Protein samples from the rhodopsin degradation assays (see below) were used to assess BEST1 levels. **(D)** GFP fluorescence in adBD iPSC-RPE transduced with lentivirus expressing hBEST1. Scale bar = 100 µm (applies to all three images). **(E)** Chloride current traces of R141H/A195V iPSC-RPE after gene augmentation measured in the presence (*black*) or absence (*gray*) of calcium. **(F-H)** Chloride current traces for adBD iPSC-RPE after gene augmentation, measured in the presence (*black*) or absence (*gray*) of calcium over a voltage ramp (-100 to +100 mV), that were used to obtain CaCC current density plots shown in Figure 2. 4.5 µM calcium was used for +calcium conditions. Cells with green fluorescence were used for all patch clamp measurements after gene augmentation. The number (n) of individual cells patch clamped in the presence or absence of calcium (in order to calculate CaCC current densities) is shown in the top left corner of each graph. Data were obtained from at least two replicates. **(I-K)** *left*, Western blots used for the rhodopsin degradation assay, *right*, and corresponding grayscale images of western blots used to quantify levels of rhodopsin shown in Figure 2 (boxes represent areas used for quantification). For each lane, the boxed area was selected to include bands corresponding to fully denatured rhodopsin and its aggregated forms.

Figure S3. Related to Figure 3

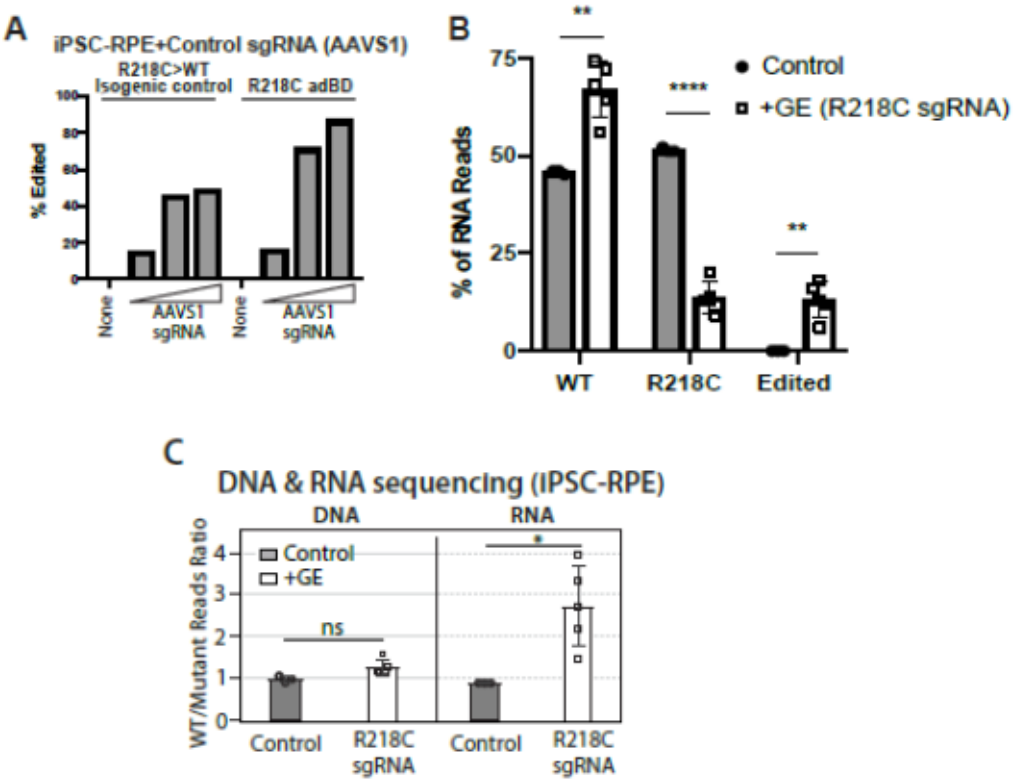

455

456

Figure S3 | Quantification of DNA and RNA sequencing reads in gene-edited (GE) iPSC-RPE. (A) Percent of *AAVS1* alleles edited (% Edited) in R218C adBD iPSC-RPE and R218C>WT isogenic control iPSC-RPE transduced with *AAVS1* sgRNA lentiviral genome editor at 0, 5, 50, or 150 µl dose. **(B)** Percent of WT, unedited R218C, or edited R218C RNA reads corresponding to Figure 3F. **(C)** Ratio of WT to total mutant (MT) allele (unedited + edited) DNA (*left*) and mRNA transcript reads (*right*) from R218C iPSC-RPE cultures treated with R218C sgRNA lentiviral genome editor (n=5) or control (n=3 for *AAVS1* lentiviral genome editor or no lentiviral genome editor). Error bars represent mean ± SD; ns = $p \geq 0.05$, * for $p < 0.05$, ** for $p < 0.01$, *** for $p < 0.001$, **** for $p < 0.0001$.

Figure S4. Related to Figure 4

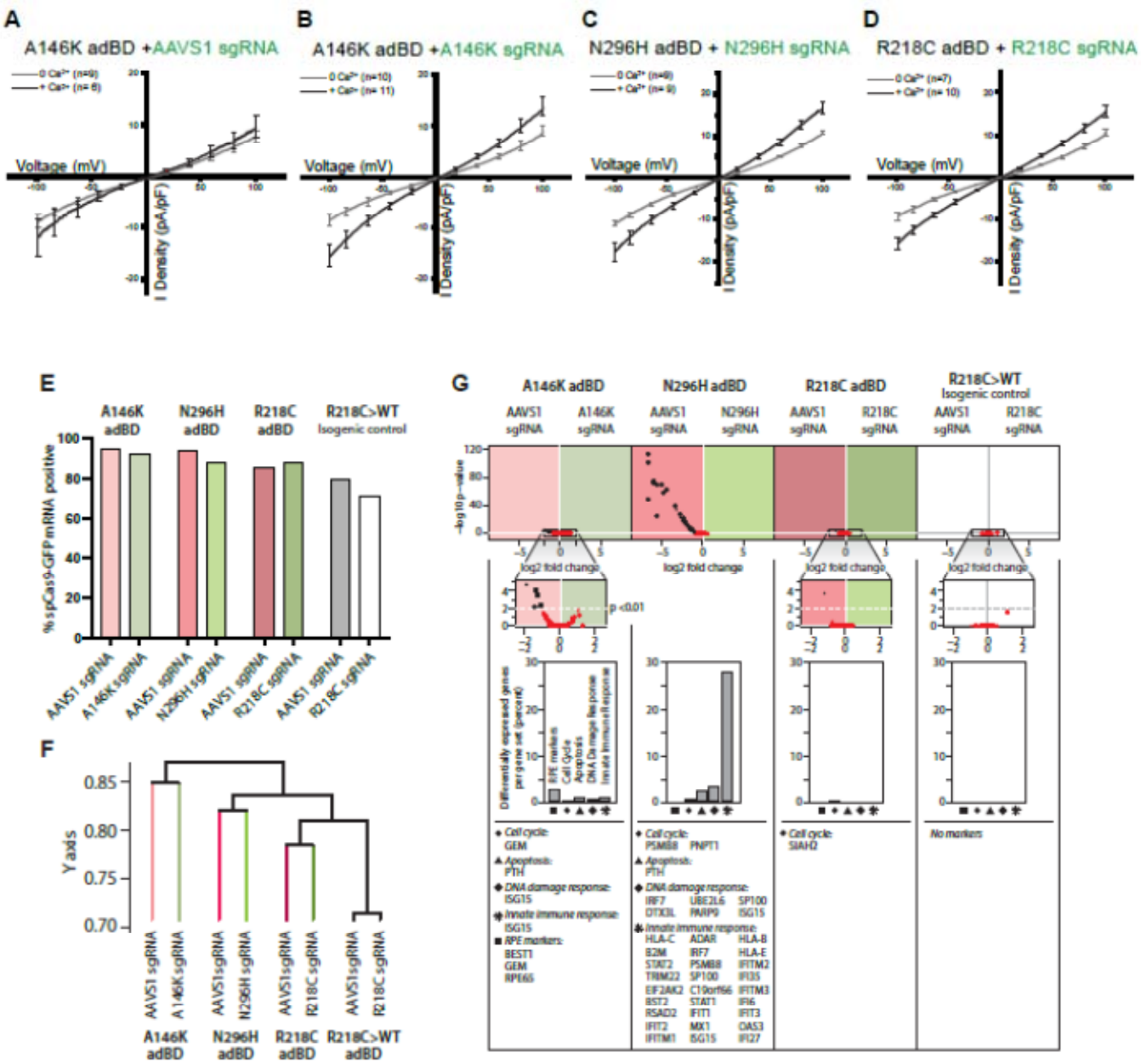

466

467

Figure S4 | Gene editing (GE) restores CaCC activity in iPSC-RPE from all tested adBD lines. (A-D) Chloride current traces, measured in the presence (*black*) or absence (*gray*) of calcium over a voltage ramp (-100 to +100 mV), that were used to calculate CaCC current density plots after gene editing of adBD iPSC-RPE. iPSC-RPE was edited using lentiviral genome editors encoding sgRNA targeting **(A)** *AAVS1* site in A146K adBD iPSC-RPE, **(B)** A146K mutation in A146K adBD iPSC-RPE, **(C)** N296H mutation in N296H adBD iPSC-RPE, or **(D)** R218C mutation in R218C adBD iPSC-RPE. Cells with GFP fluorescence were used for whole cell patch clamp measurements and 4.5 µM calcium was used for +calcium conditions. The number (n) of individual cells patch clamped with or without calcium is shown at the top left corner of each graph. Data were obtained from two replicates. **(E)** Percent of analyzed cells per sample for which *spCas9-T2A-GFP* transcripts were captured using scRNA-seq. **(F)** Dendrogram tree depicting relative similarity between samples. Non-negative matrix factorization comparison across samples indicates that greater transcriptional variability exists between iPSC-RPE lines than in the same iPSC-RPE line treated with lentiviral genome editors (*AAVS1* lentiviral genome editor versus *BEST1* mutant allele-targeted lentiviral genome editor). The dendrogram shows the similarity of the transcriptomes from each sample, derived from the average Jaccard coefficient between gene clusters from one sample and those from another sample. The y-axis denotes 1-average Jaccard coefficient and indicates the distance between different samples (tree tips) as well as between groups of samples (internal nodes). **(G)** Differential gene expression in 5 curated gene sets associated with cell cycle regulation (*circles*), apoptosis (*triangles*), DNA damage response (*diamonds*), innate immune response (*asterisks*), or RPE-identity (*squares*) in control (*AAVS1*) lentiviral genome editor versus mutant allele-targeted lentiviral genome editor treated samples. For one sample pair (N296H iPSC-RPE), genes associated with a potential adverse treatment effect were upregulated in control lentiviral genome editor-treated sample compared to the mutant allele-targeted lentiviral genome editor sgRNA-treated sample.

METHODS

CONTACT FOR REAGENT AND RESOURCE SHARING

Further information and requests for resources and reagents should be directed to and will be fulfilled by the Lead Contact, David Gamm (dgamm@wisc.edu).

EXPERIMENTAL MODEL AND SUBJECT DETAILS

iPSC lines

A total of 6 iPSC lines, 2 control and 4 patient-specific, were used in this study. In addition to one control iPSC line (normal) and two adBD patient-specific iPSC lines (A146K adBD and N296H adBD) previously used by our group for Best disease modeling (Singh et al., 2013b), we used three new iPSC lines. Two of the new iPSC lines harbored patient specific mutations: R218C for adBD and R141H/A195V for ARB. One isogenic control iPSC line was obtained by CRISPR/Cas9-based gene correction of the patient-specific R218C adBD iPSC line (Steyer et al., 2018). All iPSC lines were cultured either on mouse embryonic fibroblasts (MEFs) or on Matrigel. Lines cultured on MEFs were maintained using iPS media (Dulbecco's Modified Eagle's Medium (DMEM)/F12 (1:1), 20% Knockout Serum Replacement (KOSR), 1% MEM non-essential amino acids, 1% L-glutamine, 0.2 mM β-mercaptoethanol, 100 ng/ml FGF-2), and iPSCs cultured on Matrigel were cultured with either mTeSR1 or StemFlex media. MEFs, FGF-2, and Matrigel were purchased from WiCell (Madison, WI). All other cell culture reagents were purchased from ThermoFisher Scientific. Karyotype analysis was performed as a quality control. The manuscript does not contain human subject or animal studies, and all work with iPSC lines was carried out in accordance with institutional, national, and international guidelines and approved by the Stem Cell Research Oversight Committee at the University of Wisconsin-Madison.

METHOD DETAILS

Differentiation of iPSC lines to RPE

Differentiation of iPSCs to RPE was performed as previously described (Singh et al., 2013a; Singh et al., 2013b). Briefly, iPSCs were enzymatically lifted (1 mg/ml dispase for cells cultured on MEFs; 2 mg/ml dispase or 1 ml ReLeSR for cells cultured on Matrigel) to form aggregates, also referred to as embryoid bodies (EBs). EBs were maintained in suspension culture either in EB media (iPS media without FGF-2) and then switched to neural induction media (NIM) on day 4, or gradually weaned off mTeSR1/StemFlex and transitioned to NIM by day 4. NIM is composed of 500 ml DMEM/F12 (1:1), 1% N2 supplement, 1% MEM non-essential amino acids, 1% L-glutamine, 2 µg/ml heparin. EBs were plated on laminin (Cat# 23017015) coated 6-well plates (Nunc; Thermo Fisher Scientific) on day 7. On day 16, neural rosettes were mechanically lifted, leaving adherent cells behind that were maintained in retinal differentiation media (RDM; DMEM:F12 (3:1), 2% B27 without retinoic acid, 1% antibiotic-antimycotic solution). For the first four media changes, RDM was supplemented with 10 µM SU5402 and 3 µM CHIR99021.

After 60 days of differentiation, pigmented patches of RPE were micro-dissected, dissociated using Trypsin-EDTA (0.25%), and plated on laminin coated surfaces in RDM with 10% FBS and Rho kinase inhibitor (ROCKi; Y-27632). After 2 days, the media was changed to RDM with 2% FBS, and eventually to RDM once the cells were fully confluent. There were no differences observed between RPE differentiated from iPSCs cultured on MEFs and Matrigel. Mutant and wildtype genotypes of iPSC-RPE were verified by Sanger sequencing periodically. Heparin (Cat# H-3149) and SU5402 (Cat# SML0443-25MG) were from Sigma-Aldrich, CHIR99021 (Cat# 4423) was from Tocris Bioscience, and ReLeSR

was purchased from STEMCELL Technologies. All other differentiation reagents were purchased from ThermoFisher Scientific.

Gene expression analysis

Reverse transcriptase-PCR was used to assess RPE-specific gene expression in RPE derived from different iPSC lines as described previously (Singh et al., 2013b). Primers used are listed in Key Resources Table.

Generation of lentiviral vectors

Lentiviral plasmid with the human *VMD2* promoter driving expression of *hBEST1-T2A-GFP* was provided by Alfred S. Lewin (University of Florida). LentiCRISPR v2 (LCv2) plasmid was purchased from Addgene (Cat# 52961), and molecular cloning was used to insert specific sgRNA sequences (Table S4) as described (Steyer et al., 2018). Lentiviral gene editing plasmids containing specific sgRNA sequences and the human *VMD2* promoter driving expression of *spCas9-T2A-GFP* were then generated as described hereafter (all primers and sgRNA sequences are listed in the Key Resources Table). To begin, the '*T2A-GFP-WPRE*' sequence was amplified from the *hVMD2-hBEST1-T2A-GFP* plasmid using LCv2-GFP.Gib.F and .R primers and Q5 2X MM (NEB, Cat# M0492L). The '*2A-Puro-WPRE*' sequence was then removed from the LCv2 plasmid via restriction digestion with PmeI (NEB, Cat# R0560S) and BamHI (NEB, Cat# R3136S). The digestion product was resolved on a 0.7% agarose gel and the plasmid backbone was purified using the Monarch gel purification kit (NEB, Cat# T1020S). The '*T2A-GFP-WPRE*' sequence was inserted into the digested backbone using the Gibson Assembly kit (SGI, Cat# GA1100) per the manufacturer's instructions. The completed Gibson Assembly reaction was then amplified using chemically competent *E. coli* (NEB, Cat# C3040H) and Sanger sequenced to confirm

insertion of '*T2A-GFP-WPRE*' using LCv2-GFP.seq.L and LCv2-GFP.seq.R primers. This intermediate plasmid product (*pLCv2-GFP*) was digested with AfeI (NEB, Cat# R0652S) and EcoRI-HF (NEB, Cat R310S) to remove the constitutive EF-1 alpha core promoter. The desired digestion product was purified as described above. The *hVMD2* promoter was then PCR amplified from *hVMD2-hBEST1-T2A-GFP* using Q5 2X MM and VMD2.LCv2.GFP.Gib.F and .R primers, followed by insertion into the digested LCv2-GFP backbone via Gibson Assembly. Next, the completed Gibson reaction was transformed into chemically competent *E. coli* and the sequence of the final product *hVMD2-spCas9-T2A-GFP* was confirmed via Sanger sequencing using VMD2.LCv2.GFP.seq.L and .R primers. Subsequently, specific sgRNAs were cloned into *hVMD2-spCas9-T2A-GFP* using the same restriction digest and Gibson Assembly protocol described for generation of the LCv2 gene editing vectors.

Lentivirus production and cell transduction

Lentivirus stocks were generated by the Cell Culture Core of the UW Department of Dermatology Skin Disease Research Center (Madison, WI). Briefly, HEK293 cells cultured on 10-cm dishes were transfected with lentiviral plasmids—10 µg of sgRNA encoding lentiviral plasmid (*hVMD2-hBEST1-T2A-GFP*, *hVMD2-spCas9-T2A-GFP* or LCv2); 5 µg of psPax2 (Addgene, Cat# 12260), and 2 µg of pMD2.G (Addgene, Cat# 12259)—using Lipofectamine (ThermoFisher; Cat# 11668019). After 15 hours, culture medium (DMEM with 10% FBS) was replaced with fresh media containing 1% Penicillin-Streptomycin. Media containing lentiviruses was collected the next day and viral titers were calculated using QuickTiter Lentivirus Titer Kit (Cell Biolabs, Cat# VPK-107). Titers for lentiviral stock were:

Lentivirus	**Titer (Transduction units/ml)**
hVMD2-hBEST1-T2A-GFP	$22x10^{6-7}$
hVMD2-spCas9-T2A-GFP R218C sgRNA	$74.16\ x10^{6-7}$
hVMD2-spCas9-T2A-GFP A146K sgRNA	$74.26\ x10^{6-7}$

hVMD2-spCas9-T2A-GFP N296H sgRNA	68.91 x10^{6-7}
hVMD2-spCas9-T2A-GFP AAVS1 sgRNA	74.01 x10^{6-7}

For iPSC-RPE transduction, monolayers of iPSC-RPE on transwells were treated with 0, 5, 50, or 150 µl (Figure 3C) or 150 µl alone of specified lentivirus preparation for all other experiments. Media was changed on day 2 to RDM, and cells were maintained in culture with media changes every 3 days until used for sequencing or other analyses.

Transepithelial electrical resistance (TER) measurements

Monolayers of RPE cultured on transwell inserts (Corning, #3470) were used for all TER measurements. To perform the measurements, we employed an epithelial voltohmmeter (EVOM2) with chopstick electrodes (STX2) from World Precision Instruments (Sarasota, USA) according to manufacturer's instructions. Electrodes were sterilized with ethanol, and then rinsed in sterile Milli-Q water followed by HBSS before measuring electrical resistance of RPE monolayers. Differences between TER values of transwells with cultured RPE monolayers versus background measurements of cell-free transwell inserts were multiplied by the surface area of the transwell membrane to obtain net TER values in $\Omega \cdot cm^2$.

Calcium-activated chloride channel current density measurements

All iPSC-RPE cells used for chloride current measurements were cultured as a monolayer on transwells. To singularize cells prior to measurement, transwells were washed twice with 0 Na-CMF solution (135 mM N-Methyl-D-glucamine (NMDG)-Cl, 5 mM KCl, 10 mM HEPES, 10 mM glucose, 2 mM EDTA-KOH, pH adjusted to 7.4) and then incubated with papain enzyme solution (0 Na-CMF solution containing 2.5 µl/ml papain (46 mg/ml, MP Biomedicals LLC, Cat#100921), 0.375 mg/ml

adenosine, 0.3mg/ml L-cysteine, 0.25 mg/ml L- glutathione, and 0.05mg/ ml taurine) for 30 minutes at $37^{o}C/5\%\ CO_2$. To stop the reaction, 0.01% BSA was added to the enzymatic solution. After washing twice with 0 Na-CMF solution, cells were dispersed in extracellular solution containing 140 mM NaCl, 10 mM HEPES, 3 mM KCl, 2 mM $CaCl_2$, 2 mM $MgCl_2$, and 5.5 mM glucose adjusted to pH 7.4 with NaOH by gentle pipetting.

Cells with polarized RPE morphology post-dissociation (Figure 2B, *left*) were used to measure chloride currents. To test effects of gene augmentation or gene editing on *BEST1* mutant iPSC-RPE by single-cell patch clamp analysis, only cells with GFP fluorescence (from transduction with *hVMD2-hBEST1-T2A-GFP* for gene augmentation or *hVMD2-spCas9-T2A-GFP* encoding *AAVS1* sgRNA or mutant allele-targeted sgRNAs for gene editing) were used. Current recordings on these cells were performed using the conventional whole-cell patch clamp technique with an Axopatch 200A amplifier controlled by Clampex software program via the digidata 1550 data acquisition system (Axon Instruments, CA). Fire-polished borosilicate glass pipettes with 3-5 MΩ resistance were filled with pipette solution containing 4.5 µM calcium or no calcium.

Recordings were carried out at room temperature and current-voltage tracings were established using ramps from -100 to +100 mV for 1000 ms. The pipette solution with calcium was comprised of (in mM) 146 CsCl, 5 (Ca^{2+})-EGTA-NMDG, 2 $MgCl_2$, 8 HEPES, and 10 sucrose at pH 7.3, adjusted with NMDG. Another pipette solution devoid of calcium was comprised of (in mM) 146 CsCl, 5 EGTA-NMDG, 2 $MgCl_2$, 8 HEPES, and 10 Sucrose at pH 7.3, adjusted with NMDG. Both of these pipette solutions were mixed to make the solution containing 4.5 µM free calcium as described previously(Kuruma and Hartzell, 2000), which was then used for patch clamping.

Current density values were obtained by dividing current amplitude with cell capacitance measurements. CaCC current densities for iPSC-RPE are represented as differences between mean 4.5

μM calcium response and mean no calcium response from a total of at least five cells for each condition. At least two differentiations were used as replicates to obtain data for each line.

Immunocytochemistry

iPSC-RPE cultured on transwell inserts were washed with PBS and fixed with 4% paraformaldehyde for 10 minutes at room temperature (RT). After washing fixed cells three times with PBS, transwell membranes were placed in blocking solution (10% normal donkey serum with 5% BSA, 1% fish gelatin and 0.5% Triton-X100 in PBS) for one hour at RT, and then incubated overnight at 4 ^{o}C in primary antibody (1:100 mouse anti-Bestrophin (Millipore, Cat# MAB5466); 1:100 rabbit anti-ZO-1 (ThermoFisher Scientific, Cat# 61-7300)) prepared in blocking solution. Cells were then washed three times in PBS and incubated for 30 minutes at RT in appropriate secondary antibody (ThermoFisher Scientific; 1:500 Donkey anti-Mouse IgG (Cat# A31571); 1:500 Donkey anti-Rabbit IgG (Cat# A10040)) prepared in blocking solution. Cells were again washed three times in PBS, incubated in DAPI (1:500; ThermoFisher; Cat# D1306) for 30 minutes, mounted using prolong gold with DAPI (ThermoFisher; Cat# P36931), and imaged using Nikon A1R confocal microscope with NIS Elements AR 5.0 software.

Rhodopsin degradation assay

Photoreceptor outer segment (POS) feeding of iPSC-RPE was performed as described previously (Singh et al., 2013b). Briefly, bovine POS (InVision BioResources (Seattle, WA)) were gently resuspended in DMEM. 100 μl media was then removed from each transwell insert, 6.25×10^{6} POS were added, and cells were incubated at 37 ^{o}C and 5% CO_2 for 2 hours. Afterward, POS containing RDM was removed and each transwell was washed thoroughly three times using DPBS. Following the washes, cells were harvested (0 time point) or further incubated in fresh RDM for prescribed periods of time. At each time

point, transwells were washed, 100 µl RIPA buffer (ThermoFisher; Cat# 89900) containing protease inhibitor cocktail (Sigma-Aldrich; Cat# P8340) was added, and cells were incubated on ice for 30 minutes to extract total cell protein. Protein quantification was performed using the DC Protein assay kit II (Bio-Rad, Cat# 5000112).

Western blots were then performed to monitor rhodopsin degradation as described (Singh et al., 2015; Singh et al., 2013b). Briefly, protein lysates were denatured in 1X Laemmli buffer (reducing) and kept on ice for 10 minutes. Protein samples were then separated on 4-20% mini-Protean TGX gels (Bio-Rad; Cat# 4568095) and electroblotted onto PVDF membranes (Millipore; IPFL10100). After blotting, membranes were dried at RT for 15 minutes, re-activated in methanol for 1 minute, and then incubated in blocking buffer (1:1 Odyssey blocking buffer (LI-COR Biosciences; Cat# 927-40000):PBS) for 1 hour. Post-blocking, blots were incubated in primary antibodies (1:500 mouse anti-rhodopsin (Millipore, Cat# MABN15); 0.1 µg/ml rabbit anti-beta actin (Abcam, Cat# ab8227)) in blocking buffer with 0.1% Tween-20 overnight, washed three times for 5 minutes each in PBS with 0.1% Tween-20, incubated for 1.5 hours at RT in appropriate secondary antibody (LI-COR Biosciences; 1:20,000 Donkey anti-Rabbit IgG (Cat# 926-32213); 1:20,000 Donkey anti-Mouse IgG (Cat# 926-68022)) in blocking buffer with 0.1% Tween-20 and 0.01% SDS, and then washed three times for 5 minutes each in PBS with 0.1% Tween-20. An Odyssey infrared Imager (LI-COR Biosciences) was used to image blots using Image Studio software. ImageJ was used for quantification of relevant protein bands. Samples from rhodopsin degradation assays were also used to assess levels of BEST1 protein before and after gene augmentation. Western blots were performed as described above, using 1:1000 rabbit anti-Bestrophin1 antibody (LAgen Laboratories; Cat# 016-Best1-01) and 1:1000 mouse anti-Actin antibody (Millipore; Cat# MAB1501) as primary antibodies.

Deep sequencing analysis of DNA and RNA read frequency

Cells were singularized with TrypLE Express (Gibco, Cat# 12605010) per manufacturer's instructions. Total DNA and/or RNA was extracted using QuickExtract DNA (Epicentre, Cat# QE09050) or QuickExtract RNA (Epicentre, Cat# QER090150), respectively. Both DNA and RNA extractions were performed per manufacturer's instructions with the following minor modifications: 1) a ratio of 10,000-25,000 cells per 50 µl of QuickExtract solution was routinely used, and 2) an optional DNase 1 treatment was omitted from the RNA extraction protocol. All samples were stored at -80 ºC until use.

RNA was reverse transcribed to cDNA using the ProtoScript II First Strand synthesis kit (NEB, Cat# E6560S) and synthesis was performed with the "random primer" option included within the kit. 4 µl of crude RNA extract was added to each cDNA reaction.

In preparation for targeted deep sequencing, Illumina adapter sequences and sample-specific barcodes were appended to genomic or cDNA amplicons via overhang PCR as described (Steyer et al., 2018). Purified amplicon libraries were assembled into 2 nM total DNA in DNAse/RNAse free H_2O and sequenced using 150 nucleotide paired end reads using MiSeq (6M or 15M total reads) at the UW Biotech Center (Madison, WI) with the following loading condition: 8 pmol total DNA and 15% PhiX DNA. Raw FASTQ files were read and aligned to expected amplicons using a command line implementation of CRISPResso (v1.0.8) (Pinello et al., 2016). Full commands used for analysis are available upon request. 'Percent allele identity' or 'percent edited' were determined using the software's standard output table of individual read identities. Sequencing reads with counts <100 were not included in the analysis. All FASTQ files are available upon request.

Single-cell RNA sequencing (scRNA-seq)

iPSC-RPE cultures derived from the A146K, N296H, and R218C adBD patient lines, and from an isogenic gene-corrected control line derived from the R218C line (R218C>WT) were transduced with 150

µl of *hVMD2-spCas9-T2A-GFP* encoding specific sgRNAs as described in the 'Lentivirus production and cell transduction' section. For each sample, sgRNAs were either targeted to mutant *BEST1* or to the *AAVS1* locus (control). On day 14, cells were dissociated from transwells with a papain dissociation kit (Worthington Biochemical, Cat# LK003150) and filtered using a Flowmi cell strainer (Bel-Art SP Scienceware, Cat# H13680-0040) to obtain single-cell suspension. Cells were then prepared for scRNA-seq with the droplet-based 10X Genomics GemCode platform according to the manufacturer's instructions. In brief, singularized cells were encapsulated in oil beads containing a unique molecular identifier (UMI) barcode. The cells were then lysed and cDNA libraries were created featuring cell and transcript-specific molecular identifiers. Libraries were sequenced using an Illumina HiSeq2500 Rapid Run and reads were aligned to a custom reference genome consisting of the human hg19 GRCh38 genome and an added gene for the *spCas9-T2A-GFP* transcript.

scRNA-seq data analysis

Gene edited iPSC-RPE were clustered based on their genome-wide transcriptome using the t-Distributed Stochastic Neighbor Embedding (t-SNE) algorithm with the 10X Genomics Loupe Cell Browser software (v2.0.0). Reads for each pair of samples (*BEST1* mutant allele-targeted sgRNA vs *AAVS1* sgRNA control) were aligned, analyzed, clustered with Cell Ranger v2.1.1, and compared to detect significant differences in gene expression, with p values adjusted using the Benjamini-Hochberg correction for multiple tests. $P < 0.01$ was used as the significance threshold for all analyses. Cell Ranger using the aggregate feature was run to concatenate each pair of samples with the same genotype, and differential gene expression within each pair (with gene editing at either the *AAVS1* or *BEST1* locus) was then analyzed. Potential adverse events were probed using gene lists curated from gene ontology terms associated with the cell cycle, apoptosis, DNA damage response, and the innate immune response, as well

as a list of 149 validated marker genes associated with human RPE (Strunnikova et al., 2010) (Table S2; gene ontology sets are available on the Molecular Signatures Database <http://software.broadinstitute.org/gsea/msigdb>). Differentially-expressed genes with $p < 0.01$ were deemed to be significant. All significantly differentially-expressed genes per cluster are reported, with the exception of genes identified by Cell Ranger as having low average UMI counts. Volcano plots were generated in RStudio (v.1.1.456) using the ggplot2 package.

Non-negative matrix factorization-based comparison of scRNA-seq datasets

Non-negative matrix factorization (NMF) followed by clustering of genes using the NMF factors was used for Figure S4 to project each dataset into a gene group. The input data for this analysis were a set of gene barcode matrices generated using the Cell Ranger 2.1.1 algorithm. The matrices were filtered to remove background barcodes in order to include only detected cellular barcodes, and then further filtered to exclude cells expressing fewer than 2000 total counts, followed by depth normalization.

To enable comparison of transcriptional signatures from each sample, NMF (Lee and Seung, 2000) was applied to each scRNA-seq dataset. NMF is a popular dimensionality reduction and clustering approach that is used to project data into low dimensional non-negative factors, and thus can be used to derive a clustering of cells and genes. NMF with $k=10$ factors was applied with a total of five NMF runs. Next, the similarity of NMF results was compared between two samples using the average best Jaccard coefficient between clusters of one versus another sample. 1-average Jaccard coefficient was then used as the distance to apply hierarchical clustering on the samples. This procedure was repeated five times and the tree that appeared most often was used. The trees learned in different iterations were largely similar and always grouped the patient-specific lines first before grouping different lines together.

QUANTIFICATION AND STATISTICAL ANALYSIS

Unless otherwise specified, all analyses were performed using GraphPad Prism (v.8.0.1) and error bars represent mean ± SD; ns = $p \geq 0.05$, * for $p < 0.05$, ** for $p < 0.01$, *** for $p < 0.001$, **** for $p < 0.0001$. Further detail for each analysis is provided here. Statistical analyses for Figures 2E, 2I and 4B were performed using Origin 2018b. Student's *t*-test was performed to measure the significance between the groups. P values <0.05 were considered statistically significant. Statistical significance for Figure 4D and S3C was determined using the Holm-Sidak method with alpha = 0.05. Each row was analyzed individually, without assuming a consistent SD (number of *t* tests = 10 and 2 for Figure 4D, and S3C, respectively). Statistical significance for differential gene expression in Figures 4F and Figure S4G was determined using the Cell Ranger 2.1.1 algorithm. Sample pairs with each genotype were analyzed and clustered with individual Cell Ranger runs for each pair and analyzed using the Loupe Cell Browser (v.2.0.0). Differential expression was calculated using a negative binomial exact test, and p values were adjusted using the Benjamini-Hochberg correction for multiple tests. P <0.01 was used as the threshold for assigning significant versus non-significant changes in gene expression. Volcano plots were generated in RStudio (v 1.1.456) using the ggplot2 package. For Figures 3K, L, M, and S3B, discovery was determined using the two-stage linear step-up procedure of Benjamini, Krieger, and Yekutieli with Q = 1%. Each row was analyzed individually, without assuming a consistent SD (number of *t* tests = 3).

DATA AND SOFTWARE AVAILABILITY

Upon acceptance, scRNA-seq data will be posted to an accession database. Raw targeted sequencing files for DNA and RNA sequencing data will be deposited to the NCBI Trace and Short-Read Archive. Raw patch clamp data are available upon request. Other experimental data are provided in Supplemental files and all source data are available upon request.

761 **KEY RESOURCES TABLE**

REAGENT or RESOURCE	SOURCE	IDENTIFIER
Antibodies		
Mouse anti-Bestrophin	Millipore	Cat# MAB5466
Rabbit anti-Bestrophin	LAgen Laboratories	Cat# 016-Best1-01
Rabbit anti-ZO-1	Thermo Fisher Scientific	Cat# 61-7300
Donkey anti-mouse IgG	Thermo Fisher Scientific	Cat# A31571
Donkey anti-Rabbit IgG	Thermo Fisher Scientific	Cat# A10040
Mouse anti-rhodopsin	Millipore	Cat# MABN15
Rabbit anti-beta actin	Abcam	Cat# ab8227
Mouse anti-Actin	Millipore	Cat# MAB1501
Donkey anti-rabbit IgG	LI-COR Biosciences	Cat# 926-32213
Donkey anti-mouse IgG	LI-COR Biosciences	Cat# 926-68022
Bacterial and Virus Strains		
LV-hVMD2-hBEST1-T2A-GFP (Lentivirus)	Alfred S. Lewin, University of Florida Manufactured by Cell culture Core, UW Department of Dermatology Skin Disease Research Center (SDRC)	N/A
LV-spCas9-sgRNA-T2A-GFP with allele-specifc gRNA	This paper Manufactured by SDRC	N/A
Biological Samples		
N/A	N/A	N/A
Chemicals, Peptides, and Recombinant Proteins		
N-methyl-D-glucamine (NMDG)	Sigma- Aldrich	Cat# M2004
Sodium Chloride (NaCl)	Sigma- Aldrich	Cat# 746398
Potassium Chloride (KCl)	Sigma- Aldrich	Cat# P3911
Calcium Chloride ($CaCl_2$)	Sigma- Aldrich	Cat# C1016
HEPES	Sigma- Aldrich	Cat# H3375
Glucose	Sigma- Aldrich	Cat# G8270
EDTA	Sigma- Aldrich	Cat# EDS
L-Cysteine	Sigma- Aldrich	Cat# C7352
L-Glutathione	Sigma- Aldrich	Cat# G4251
Taurine	Sigma- Aldrich	Cat# T0625
Adenosine	Sigma- Aldrich	Cat# A9251
Bovine Serum Albumin (BSA)	Sigma- Aldrich	Cat# A7906
Papain	MP Biomedicals LLC	Cat# 100921
Cesium Chloride (CsCl)	MP Biomedicals LLC	Cat# 101321
Magnesium Chloride ($MgCl_2$)	Sigma- Aldrich	Cat# M8266
Sucrose	Sigma- Aldrich	Cat# S7903
EGTA	Fisher Chemicals	Cat# 02783
Sodium Hydroxide (NaOH)	Fisher Chemicals	Cat# S318
FGF-2	WiCell (Madison, WI)	N/A
Matrigel	WiCell (Madison, WI)	N/A
Dulbecco's Modified Eagle's Medium (DMEM/F12)	Gibco	Cat# 11320082
Knockout Serum Replacement (KOSR)	WiCell (Madison, WI)	N/A
MEM non-essential amino acids	Gibco	Cat# 11140050

L-glutamine	Gibco	Cat# 25030081
mTESR1	WiCell (Madison, WI)	N/A
StemFlex Medium	Gibco	Cat# A3349401
ß-Mercaptoethanol	Sigma-Aldritch	Cat# M3148
Dispase	Gibco	Cat# 17105041
ReLeSR	Stemcell Technologies	Cat# 05872
N2 supplement	Gibco	Cat# 17502001
Heparin	Sigma-Aldritch	Cat# H-3149
Laminin	Thermo Fisher Scientific	Cat# 23017015
B27 without retinoic acid	Gibco	Cat# 12587010
Antibiotic-antimycotic solution	Gibco	Cat# 15240062
SU5402	Sigma-Aldritch	Cat# SML0443-25MG
CHIR99021	Tocris Bioscience	Cat# 4423
Trypsin-EDTA	Gibco	Cat# 25300054
Rho kinase inhibitor (ROCKi)	SelleckChem	Cat# Y-27632
Q5 2X Master Mix	New England Biolabs	Cat# M0492L
PmeI	New England Biolabs	Cat# R0560S
BamHI	New England Biolabs	Cat# R3136S
AfeI	New England Biolabs	Cat# R0652S
EcoRI-HF	New England Biolabs	Cat# R310S
Lipofectamine 2000	Thermo Fisher	Cat# 11668019
DMEM	Gibco	Cat# 11965092
FBS	WiCell (Madison, WI)	N/A
Penicillin-streptomycin	Gibco	Cat# 15140122
Phosphate Buffered Saline (PBS)	Gibco	Cat# 14190144
Formaldehyde	Sigma- Aldrich	Cat# 47608
Normal Donkey Serum	Sigma- Aldrich	Cat# D9663-10ML
Fish Gelatin	Sigma- Aldrich	Cat# G7041
Triton-X100	Sigma- Aldrich	Cat# T8787
DAPI	Thermo Fisher Scientific	Cat# D1306
Prolong gold with DAPI	Thermo Fisher Scientific	Cat# P36931
Bovine Photoreceptor Outer Segments (POS)	InVision BioResources	Cat# 98740
RIPA Buffer	Thermo Fisher Scientific	Cas# 89900
Protease inhibitor cocktail	Sigma-Aldrich	Cat# P8340
Odyssey blocking buffer	LI-COR Bioscienes	Cat# 927-40000
Tween-20	Sigma- Aldrich	Cat# P7949
SDS	Sigma- Aldrich	Cat# L3771
TrypLE Express	Gibco	Cat# 12605010
QuickExtract DNA	Epicentre	Cat# QE09050
QuickExtract RNA	Epicentre	Cat# QER090150
DNase 1	Invitrogen	Cat# 18047019
Critical Commercial Assays		
Monarch Gel Purification Kit	New England Biolabs	Cat# T1020S
Gibson Assembly Kit	SGI	Cat# GA1100
QuickTiter Lentivirus Titer Kit	Cell Biolabs	Cat# VPK-107

DC Protein Assay Kit II	BioRad	Cat# 5000112
4-20% mini-Protean TGX gel	BioRad	Cat# 4568095
PVDF membrane	Millipore	Cat# IPFL10100
ProtoScript II First Strand Synthesis Kit	New England Biolabs	Cat# E6560S
Papain dissociation kit	Worthington Biochemical	Cat# LK003150
Chromium single cell 3' library and gel bead kit (V2 chemistry)	10X Genomics	Cat# 1000092
Deposited Data		
scRNA-seq data.	Will post to accession database upon acceptance.	Pending
Raw targeted sequencing files for DNA and RNA sequencing data and raw patch clamp data	Available upon request.	N/A
All other experimental data are provided in the source data files or in supplement.	N/A	N/A
Experimental Models: Cell Lines		
Cell line: iPSC – *Best1*$^{WT/WT}$ *Normal*	Singh et al., 2013b	N/A
Cell line: iPSC – *Best1*$^{WT/WT}$ isogenic to *Best1*$^{R218C/WT}$	Steyer et al. 2018	N/A
Cell line: iPSC – *Best1*$^{R218C/WT}$	Steyer et al. 2018	N/A
Cell line: iPSC – *Best1*$^{N296H/WT}$	Singh et al. 2013b	N/A
Cell line: iPSC – *Best1*$^{A146K/WT}$	Singh et al. 2013b	N/A
Cell line: iPSC – *Best1*$^{R141H/A195V}$	This paper; from Budd Tucker and Ed Stone, University of Iowa	N/A
Mouse Embryonic Fibroblasts	WiCell (Madison, WI)	N/A
Human Embryonic Kidney Cells (HEK293)	SDRC (Madison, WI)	N/A
Oligonucleotides		
BEST1 RT-PCR FWD primer: ATTTATAGGCTGGCCCTCACGGAA	Singh et al. 2013b	N/A
BEST1 RT-PCR REV primer: TGTTCTGCCGGAGTCATAAAGCCT	Singh et al. 2013b	N/A
MITF RT-PCR FWD primer: TTCACGAGCGTCCTGTATGCAGAT	Singh et al. 2013b	N/A
MITF RT-PCR REV primer: TTGCAAAGCAGGATCCATCAAGCC	Singh et al. 2013b	N/A
PEDF RT-PCR FWD primer: AATCCATCATTCACCGGGCTCTCT	Singh et al. 2013b	N/A
PEDF RT-PCR REV primer: TGCACCCAGTTGTTGATCTCTTGC	Singh et al. 2013b	N/A
RPE65 RT-PCR FWD primer: GCCCTCCTGCACAAGTTTGACTTT	Singh et al. 2013b	N/A
RPE65 RT-PCR REV primer: AGTTGGTCTCTGTGCAAGCGTAGT	Singh et al. 2013b	N/A
OCCLUDIN RT-PCR FWD primer: TCATTGCCGCGTTGGTGATCTTTG	Singh et al. 2013b	N/A
OCCLUDIN RT-PCR REV primer: ATGATGCCCAGGATAGCACTCACT	Singh et al. 2013b	N/A
CRALBP RT-PCR FWD primer: TTCCGCATGGTACCTGAAGAGGAA	Singh et al. 2013b	N/A

CRALBP RT-PCR REV primer: ACTGCAGCCGGAAATTCACATAGC	Singh et al. 2013b	N/A
GAPDH RT-PCR FWD primer: CAACGGATTTGGTCGTATTGG	Singh et al. 2013b	N/A
GAPDH RT-PCR REV primer: GCAACAATATCCACTTTACCACAGTTAA	Singh et al. 2013b	N/A
Cloning primer: LCv2-GFP.Gib.F GATTACAAAGACGATGACGATAAGGGATCCGGTGAGGGCAGAGGAAGTC	This paper	N/A
Cloning primer: LCv2-GFP.Gib.R ACAGTCGAGGCTGATCAGCGGGTTTAAACCTACTACTGCTAGAGATTTTCCACAC	This paper	N/A
Cloning primer: LCv2-GFP.seq.L ACCGGCCTGTACGAGACACG	This paper	N/A
Cloning primer: LCv2-GFP.seq.R GAAAGGACAGTGGGAGTGGCACC	This paper	N/A
Cloning primer: VMD2.LCv2.GFP.Gib.F GTGGCACCGAGTCGGTGCTTTTTTGAATTCCAATTCTGTCATTTTACTAGGGTGATGAAATTC	This paper	N/A
Cloning primer: VMD2.LCv2.GFP.Gib.R TGTACTTCTTGTCCATGGTGGCAGCGCTCTATCGGCCGCGGGTACA	This paper	N/A
Cloning primer: VMD2.LCv2.GFP.seq.L GAATGAATACCGGGCTGCAGTCAAC	This paper	N/A
Cloning primer: VMD2.LCv2.GFP.seq.R GTCGGTGATCACGGCCCAG	This paper	N/A
Deep Sequencing Primer: MT.C.OT.5v2.HTS.F GTTGGTTCCTGAAGATGGGCAG	This paper	N/A
Deep Sequencing Primer: MT.C.OT.5v2.HTS.R CTGTCAAGGCCAAGTTCTGCTG	This paper	N/A
Deep Sequencing Primer: MT.C.OT.2.HTS.F GCTAAATTCTGCTATAAAAGGAAGG	This paper	N/A
Deep Sequencing Primer: MT.C.OT.2.HTS.R GCATTGCTTTAGAAAACTCAGAAGT	This paper	N/A
Deep Sequencing Primer: MT.C.OT.3.HTS.F AGTGAGACCAAGTTCTGACAGCA	This paper	N/A
Deep Sequencing Primer: MT.C.OT.3.HTS.R GGCCTCTTCATACATACACATGCAC	This paper	N/A
Deep Sequencing Primer: MT.C.OT.4.HTS.F CCTCCACATCTGCAGAAAAGTGT	This paper	N/A
Deep Sequencing Primer: MT.C.OT.4.HTS.R GGCAGGGTTTGGTCTCCTACTT	This paper	N/A
Deep Sequencing Primer: MT.C.OT.5.HTS.F GGATGGCTCTGGGTGGGTTT	This paper	N/A
Deep Sequencing Primer: MT.C.OT.5.HTS.R CTTCCAACTCTTCCTCCCACCC	This paper	N/A
Deep Sequencing Primer: MT.C.OT.6.HTS.F TGAGGTTCAGAATAGCTCAGCA	This paper	N/A

Deep Sequencing Primer: MT.C.OT.6.HTS.R TGTTTCTGTGAAGCAAATCAAAGCT	This paper	N/A
Deep Sequencing Primer: MT.C.OT.7.HTS.F TGTTTCTGTGAAGCAAATCAAAGCT	This paper	N/A
Deep Sequencing Primer: MT.C.OT.7.HTS.R TGAGGTTCAGAATAGCTCAGCA	This paper	N/A
Deep Sequencing Primer: MT.C.OT.8.HTS.F AAAGCATGGCGGGAGTGCTAA	This paper	N/A
Deep Sequencing Primer: MT.C.OT.8.HTS.R TGACTAAATCCCTGGCATCGCT	This paper	N/A
Deep Sequencing Primer: MT.C.OT.9.HTS.F GCCAGTAATTTTCCAAGGCTTCT	This paper	N/A
Deep Sequencing Primer: MT.C.OT.9.HTS.R TTCCTACTAGAACCTCCTTGAG	This paper	N/A
Deep Sequencing Primer: MT.C.OT.10.HTS.F GTGACCTGACTTTGCTGAAAGGT	This paper	N/A
Deep Sequencing Primer: MT.C.OT.10.HTS.R ACCTGAATTATCTCAAGCTCACT	This paper	N/A
Deep Sequencing Primer: AAVS1T2.HTS.F ATGTGGCTCTGGTTCTGGGTAC	This paper	N/A
Deep Sequencing Primer: AAVS1T2.HTS.R GAGACTAGGAAGGAGGAGGCCT	This paper	N/A
Deep Sequencing Primer: R218C.HTSv2.F GTGTTCAGAACCCCATCCCC	This paper	N/A
Deep Sequencing Primer: R218C.HTSv2.R AGCCTAGTCCTCACCTGTGT	This paper	N/A
Deep Sequencing Primer: BEST.cDNA.HTSv2.F GGTCGAATCCGGGACCCTATC	This paper	N/A
Deep Sequencing Primer: BEST.cDNA.HTSv2.R GCCACAGTCACCACCTGTGTAT	This paper	N/A
Deep Sequencing Primer: AAVS1T2.HTS.F ATGTGGCTCTGGTTCTGGGTAC	This paper	N/A
Deep Sequencing Primer: AAVS1T2.HTS.R GAGACTAGGAAGGAGGAGGCCT	This paper	N/A
Recombinant DNA		
Plasmid: LCv2.*AAVS1* sgRNA: GGGGCCACTAGGGACAGGAT	This paper; backbone is LentiCRISPR v2. Sanjana et al. 2014	N/A
Plasmid: LCv2.R218C sgRNA: GTGTCCACACTGAGTACACA	This paper; backbone is LentiCRISPR v2. Sanjana et al. 2014	N/A
Plasmid: LCv2.WT sgRNA: GTGTCCACACTGAGTACGCA	This paper; backbone is LentiCRISPR v2. Sanjana et al. 2014	N/A
Plasmid: VMD2.*AAVS1* sgRNA: GGGGCCACTAGGGACAGGAT	This paper; backbone is hVMD2-spCas9-T2A-GFP (Alfred Lewin, University of Florida)	N/A

Plasmid: VMD2.R218C sgRNA: GTGTCCACACTGAGTACACA	This paper; backbone is hVMD2-spCas9-T2A-GFP (Alfred Lewin, University of Florida)	N/A
Plasmid: VMD2.WT sgRNA: GTGTCCACACTGAGTACGCA	This paper; backbone is hVMD2-spCas9-T2A-GFP (Alfred Lewin, University of Florida)	N/A
Plasmid: VMD2.N296H sgRNA: CATCATCCTCTCCAAAGGGG	This paper; backbone is hVMD2-spCas9-T2A-GFP (Alfred Lewin, University of Florida)	N/A
Plasmid: VMD2.A146K sgRNA: CTTTGGTGCTGACGCTGCGC	This paper; backbone is hVMD2-spCas9-T2A-GFP (Alfred Lewin, University of Florida)	N/A
psPax2	Addgene	Cat # 12260
pMD2.G	Addgene	Cat# 12259
LentiCRISPR v2	Addgene	Cat# 52961
Software and Algorithms		
Clampex 10.7	Molecular Devices, LLC	https://www.moleculardevices.com/
Clampfit 10.7	Molecular Devices, LLC	https://www.moleculardevices.com/
Origin 2018b	OriginLab Corporation	www.OriginLab.com
NIS Elements AR v4.5, NIS Elements AR v5.0, NIS Elements D v3.26, NIS Elements D v5.0	Nikon Instruments	https://www.nikoninstruments.com/Products/Software
ImageStudio 5.2	LI-COR Biosciences	https://www.licor.com/bio/image-studio/
Ca-EGTA calculator v1.3	Theo Schoenmakers' Chelator	http://web.stanford.edu/~cpatton/CaEGTA-TS.htm
ImageJ	Schneider et al., 2012	https://imagej.nih.gov/ij/
CRISPResso v1.0.8	Pinello et al. 2016	http://crispresso.rocks/help
Cell Ranger v2.1.1	10X Genomics	https://support.10xgenomics.com
Loupe Cell Browser v2.0.0	10X Genomics	https://support.10xgenomics.com
RStudio v1.1.465	Foundation for Open Access Statistics	https://github.com/rstudio
ggplot2	Wickham et al. 2010	https://github.com/tidyverse/ggplot2
GraphPad Prism	GraphPad	https://www.graphpad.com/scientific-software/prism/
Other		
Borosilicate Glass with Filament	Sutter Instruments	Cat# BF 150-117-10
Transwell Inserts	Corning	Cat# 3470

Flowmi cell strainer	Bel-Art SP Scienceware	Cat# H13680-0040

REFERENCES

Bakondi, B., Lv, W.J., Lui, B., Jones, M.K., Tsai, Y., Kim, K.J., Levy, R., Akhtar, A.A., Breunig, J.J., Svendseni, C.N., *et al.* (2016). In Vivo CRISPR/Cas9 Gene Editing Corrects Retinal Dystrophy in the S334ter-3 Rat Model of Autosomal Dominant Retinitis Pigmentosa. Mol Ther *24*, 556-563.

Boon, C.J., Klevering, B.J., Leroy, B.P., Hoyng, C.B., Keunen, J.E., and den Hollander, A.I. (2009). The spectrum of ocular phenotypes caused by mutations in the BEST1 gene. Prog Retin Eye Res *28*, 187-205.

Courtney, D.G., Moore, J.E., Atkinson, S.D., Maurizi, E., Allen, E.H., Pedrioli, D.M., McLean, W.H., Nesbit, M.A., and Moore, C.B. (2016). CRISPR/Cas9 DNA cleavage at SNP-derived PAM enables both in vitro and in vivo KRT12 mutation-specific targeting. Gene Ther *23*, 108-112.

Cideciyan, A.V., Sudharsan, R., Dufour, V.L., Massengill, M.T., Iwabe, S., Swider, M., Lisi, B., Sumaroka, A., Marinho, L.F., Appelbaum, T., Rossmiller, B., Hauswirth, W.W., Jacobson, S.G., Lewin, A.S., Aguirre, G.D., Beltran, W.A. (2018) Mutation-independent rhodopsin gene therapy by knockdown and replacement with a single AAV vector. Proc Natl Acad Sci U S A *115*(36), E8547-E8556.

Cox, D.B., Platt, R.J., and Zhang, F. (2015). Therapeutic genome editing: prospects and challenges. Nat Med *21*, 121-131.

Cromer, M.K., Vaidyanathan, S., Ryan, D.E., Curry, B., Lucas, A.B., Camarena, J., Kaushik, M., Hay, S.R., Martin, R.M., Steinfeld, I., *et al.* (2018). Global Transcriptional Response to CRISPR/Cas9-AAV6-Based Genome Editing in CD34(+) Hematopoietic Stem and Progenitor Cells. Mol Ther *26*, 2431-2442.

Cukras, C., Wiley, H.E., Jeffrey, B.G., Sen, H.N., Turriff, A., Zeng, Y., Vijayasarathy, C., Marangoni, D., Ziccardi, L., Kjellstrom, S., *et al.* (2018). Retinal AAV8-RS1 Gene Therapy for X-Linked Retinoschisis: Initial Findings from a Phase I/IIa Trial by Intravitreal Delivery. Mol Ther *26*, 2282-2294.

Dickson, V.K., Pedi, L., and Long, S.B. (2014). Structure and insights into the function of a Ca2+-activated Cl- channel. Nature *516*, 213-218.

Doudna, J.A., and Charpentier, E. (2014). The new frontier of genome engineering with CRISPR-Cas9. Science *346*, 1077-+.

George, A.L., Jr. (2004). Inherited Channelopathies Associated with Epilepsy. Epilepsy Curr *4*, 65-70.

Guziewicz, K.E., Cideciyan, A.V., Beltran, W.A., Komaromy, A.M., Dufour, V.L., Swider, M., Iwabe, S., Sumaroka, A., Kendrick, B.T., Ruthel, G., *et al.* (2018). BEST1 gene therapy corrects a diffuse retina-wide microdetachment modulated by light exposure. P Natl Acad Sci USA *115*, E2839-E2848.

Guziewicz, K.E., Sinha, D., Gomez, N.M., Zorych, K., Dutrow, E.V., Dhingra, A., Mullins, R.F., Stone, E.M., Gamm, D.M., Boesze-Battaglia, K., *et al.* (2017). Bestrophinopathy: An RPE-photoreceptor interface disease. Prog Retin Eye Res *58*, 70-88.

Johnson, A.A., Guziewicz, K.E., Lee, C.J., Kalathur, R.C., Pulido, J.S., Marmorstein, L.Y., and Marmorstein, A.D. (2017). Bestrophin 1 and retinal disease. Prog Retin Eye Res *58*, 45-69.

Johnson, A.A., Lee, Y.S., Chadburn, A.J., Tammaro, P., Manson, F.D., Marmorstein, L.Y., and Marmorstein, A.D. (2014). Disease-causing mutations associated with four bestrophinopathies exhibit disparate effects on the localization, but not the oligomerization, of Bestrophin-1. Exp Eye Res *121*, 74-85.

Kosicki, M., Tomberg, K., and Bradley, A. (2018). Repair of double-strand breaks induced by CRISPR-Cas9 leads to large deletions and complex rearrangements. Nat Biotechnol *36*, 765-771.

Kuruma, A., and Hartzell, H.C. (2000). Bimodal control of a Ca(2+)-activated Cl(-) channel by different Ca(2+) signals. J Gen Physiol *115*, 59-80.

Lam, B.L., Davis, J.L., Gregori, N.Z., MacLaren, R.E., Girach, A., Verriotto, J.D., Rodriguez, B., Rosa, P.R., Zhang, X., and Feuer, W.J. (2019). Choroideremia Gene Therapy Phase 2 Clinical Trial: 24-Month Results. Am J Ophthalmol *197*, 65-73.

Ledford, H. (2017). FDA advisers back gene therapy for rare form of blindness. Nature *550*, 314.

Lee, D.D., and Seung, H.S. (2000). Algorithms for Non-negative Matrix Factorization. Advances in Neural Information Processing Systems *13*, 556-562.

Li, P., Kleinstiver, B.P., Leon, M.Y., Prew, M.S., Navarro-Gomez, D., Greenwald, S.H., Pierce, E.A., Joung, J.K., Liu, Q. (2018). Allele-Specific CRISPR-Cas9 Genome Editing of the Single-Base P23H Mutation for Rhodopsin-Associated Dominant Retinitis Pigmentosa. The CRISPR Journal *1*, 55-64.

Li, Y., Zhang, Y., Xu, Y., Kittredge, A., Ward, N., Chen, S., Tsang, S.H., and Yang, T. (2017). Patient-specific mutations impair BESTROPHIN1's essential role in mediating Ca(2+)-dependent Cl(-) currents in human RPE. Elife *6*.

Mali, P., Yang, L., Esvelt, K.M., Aach, J., Guell, M., DiCarlo, J.E., Norville, J.E., and Church, G.M. (2013). RNA-guided human genome engineering via Cas9. Science *339*, 823-826.

Marmorstein, A.D., Johnson, A.A., Bachman, L.A., Andrews-Pfannkoch, C., Knudsen, T., Gilles, B.J., Hill, M., Gandhi, J.K., Marmorstein, L.Y., and Pulido, J.S. (2018). Mutant Best1 Expression and Impaired Phagocytosis in an iPSC Model of Autosomal Recessive Bestrophinopathy. Sci Rep *8*, 4487.

Milenkovic, A., Milenkovic, V.M., Wetzel, C.H., and Weber, B.H.F. (2018). BEST1 protein stability and degradation pathways differ between autosomal dominant Best disease and autosomal recessive bestrophinopathy accounting for the distinct retinal phenotypes. Hum Mol Genet *27*, 1630-1641.

Pattanayak, V., Lin, S., Guilinger, J.P., Ma, E., Doudna, J.A., and Liu, D.R. (2013). High-throughput profiling of off-target DNA cleavage reveals RNA-programmed Cas9 nuclease specificity. Nat Biotechnol *31*, 839-843.

Pawan K. Shahi, D.H., Divya Sinha, Simran Brar, Hannah Moulton, Sabrina Stulo, Katarzyna D. Borys, Elizabeth Capowski, De-Ann M. Pillers, David M. Gamm, Bikash R. Pattnaik (2019). Gene augmentation and read-through rescue channelopathy in an iPSC-RPE model of congenital blindness. American Journal of Human Genetics.

Pinello, L., Canver, M.C., Hoban, M.D., Orkin, S.H., Kohn, D.B., Bauer, D.E., and Yuan, G.C. (2016). Analyzing CRISPR genome-editing experiments with CRISPResso. Nat Biotechnol *34*, 695-697.

Popp, M.W., and Maquat, L.E. (2016). Leveraging Rules of Nonsense-Mediated mRNA Decay for Genome Engineering and Personalized Medicine. Cell *165*, 1319-1322.

Russell, S., Bennett, J., Wellman, J.A., Chung, D.C., Yu, Z.F., Tillman, A., Wittes, J., Pappas, J., Elci, O., McCague, S.*, et al.* (2017). Efficacy and safety of voretigene neparvovec (AAV2-hRPE65v2) in patients with RPE65-mediated inherited retinal dystrophy: a randomised, controlled, open-label, phase 3 trial. Lancet *390*, 849-860.

Sadelain, M., Papapetrou, E.P., and Bushman, F.D. (2011). Safe harbours for the integration of new DNA in the human genome. Nat Rev Cancer *12*, 51-58.

Schaaf, C.P. (2014). Nicotinic acetylcholine receptors in human genetic disease. Genet Med *16*, 649-656.

Shen, M.W., Arbab, M., Hsu, J.Y., Worstell, D., Culbertson, S.J., Krabbe, O., Cassa, C.A., Liu, D.R., Gifford, D.K., and Sherwood, R.I. (2018). Predictable and precise template-free CRISPR editing of pathogenic variants. Nature *563*, 646-651.

Singh, R., Kuai, D., Guziewicz, K.E., Meyer, J., Wilson, M., Lu, J., Smith, M., Clark, E., Verhoeven, A., Aguirre, G.D.*, et al.* (2015). Pharmacological Modulation of Photoreceptor Outer Segment Degradation in a Human iPS Cell Model of Inherited Macular Degeneration. Mol Ther *23*, 1700-1711.

Singh, R., Phillips, M.J., Kuai, D., Meyer, J., Martin, J.M., Smith, M.A., Perez, E.T., Shen, W., Wallace, K.A., Capowski, E.E.*, et al.* (2013a). Functional analysis of serially expanded human iPS cell-derived RPE cultures. Invest Ophthalmol Vis Sci *54*, 6767-6778.

Singh, R., Shen, W., Kuai, D., Martin, J.M., Guo, X.R., Smith, M.A., Perez, E.T., Phillips, M.J., Simonett, J.M., Wallace, K.A.*, et al.* (2013b). iPS cell modeling of Best disease: insights into the pathophysiology of an inherited macular degeneration. Hum Mol Genet *22*, 593-607.

Steyer, B., Bu, Q., Cory, E., Jiang, K., Duong, S., Sinha, D., Steltzer, S., Gamm, D., Chang, Q., and Saha, K. (2018). Scarless Genome Editing of Human Pluripotent Stem Cells via Transient Puromycin Selection. Stem Cell Reports *10*, 642-654.

Strunnikova, N.V., Maminishkis, A., Barb, J.J., Wang, F., Zhi, C., Sergeev, Y., Chen, W., Edwards, A.O., Stambolian, D., Abecasis, G.*, et al.* (2010). Transcriptome analysis and molecular signature of human retinal pigment epithelium. Hum Mol Genet *19*, 2468-2486.

Tsai, Y.T., Wu, W.H., Lee, T.T., Wu, W.P., Xu, C.L., Park, K.S., Cui, X., Justus, S., Lin, C.S., Jauregui, R.*, et al.* (2018). Clustered Regularly Interspaced Short Palindromic Repeats-Based Genome Surgery for the Treatment of Autosomal Dominant Retinitis Pigmentosa. Ophthalmology *125*, 1421-1430.

Vasireddy, V., Mills, J.A., Gaddameedi, R., Basner-Tschakarjan, E., Kohnke, M., Black, A.D., Alexandrov, K., Zhou, S., Maguire, A.M., Chung, D.C.*, et al.* (2013). AAV-mediated gene therapy for choroideremia: preclinical studies in personalized models. PLoS One *8*, e61396.

Villa, C., and Combi, R. (2016). Potassium Channels and Human Epileptic Phenotypes: An Updated Overview. Front Cell Neurosci *10*, 81.

Waugh, N., Loveman, E., Colquitt, J., Royle, P., Yeong, J.L., Hoad, G., and Lois, N. (2018). Treatments for dry age-related macular degeneration and Stargardt disease: a systematic review. Health Technol Assess *22*, 1-168.

Wienert, B., Shin, J., Zelin, E., Pestal, K., and Corn, J.E. (2018). In vitro-transcribed guide RNAs trigger an innate immune response via the RIG-I pathway. PLoS Biol *16*, e2005840.

Yang, T., Liu, Q., Kloss, B., Bruni, R., Kalathur, R.C., Guo, Y., Kloppmann, E., Rost, B., Colecraft, H.M., and Hendrickson, W.A. (2014). Structure and selectivity in bestrophin ion channels. Science *346*, 355-359.

SUPPLEMENTAL DATA

Supplemental Figures:

Figure S1. Characterization of iPSC-RPE.

Figure S2. Gene augmentation (GA) restores CaCC function in ARB iPSC-RPE and R218C and N296H adBD iPSC-RPE, but not in A146K adBD iPSC-RPE.

Figure S3. Quantification of DNA and RNA sequencing reads in gene-edited (GE) iPSC-RPE.

Figure S4. Gene editing (GE) restores CaCC activity in iPSC-RPE from all tested adBD lines.

Supplemental Tables:

Table S1. Frameshift analysis of iPSC-RPE+GE.

Table S2: Curated gene sets used to assess differences in gene expression between control (*AAVS1*) and MT *BEST1* allele-targeted sgRNA in Figure S4.

Table S3. Ranked off-target sites for sgRNAs used in this study

Table S4. Analysis of additional adBD mutations for amenability to allele specific editing or scarless base editing.